TITLE

Alloreactivity and autoreactivity converge to support B cell epitope targeting in transplant rejection

AUTHORS

Killian JT, Jr.,[1,*] King RG,[2] Kizziah JL,[2] Fucile CF,[3] Diaz-Avalos R,[4] Qiu S,[2] Silva-Sanchez A,[5] Mousseau BJ,[2] Macon KJ,[2] Callahan AR,[2] Yang G,[2] Hossain ME,[5] Akther J,[2] Houp JA,[1] Rosenblum FD,[6] Porrett PM,[1] Ong SC,[7] Kumar V,[7] Mobley JA,[8] Saphire EO,[4] Kearney JF,[2] Randall TD,[5] Rosenberg AF,[2,3] Green TJ,[2] Lund FE[2,9,*]

AUTHOR AFFILIATIONS

[1]Department of Surgery, University of Alabama at Birmingham Heersink School of Medicine, Birmingham, AL 35294, USA
[2]Department of Microbiology, University of Alabama at Birmingham Heersink School of Medicine, Birmingham, AL 35294, USA
[3]Informatics Institute, The University of Alabama at Birmingham, Birmingham, AL 35294, USA
[4]Center for Infectious Disease and Vaccine Discovery, La Jolla Institute for Immunology, La Jolla, CA 92037, USA
[5]Department of Medicine, Division of Clinical Immunology and Rheumatology, University of Alabama at Birmingham Heersink School of Medicine, Birmingham, AL 35294, USA
[6]Department of Pathology, University of Alabama at Birmingham Heersink School of Medicine, Birmingham, AL 35294, USA
[7]Department of Medicine, Division of Nephrology, University of Alabama at Birmingham Heersink School of Medicine, Birmingham, AL 35294, USA
[8]Department of Anesthesiology, University of Alabama at Birmingham Heersink School of Medicine, Birmingham, AL 35294, USA
[9]Lead contact

*Correspondence: john.t.killian@gmail.com (J.T.K.), flund@uab.edu (F.E.L.)

ABSTRACT

Antibody (Ab) responses against human leukocyte antigen (HLA) proteins mismatched between donor and recipient are leading cause of allograft loss in kidney transplantation. However, therapies targeting alloreactive B cell and Ab-secreting cell (ASC) are lacking, motivating the need to understand how to prevent and abrogate these alloresponses. Using molecular, structural, and proteomic techniques, we profiled the B cell response in a kidney transplant recipient with antibody-mediated rejection and graft loss. We found that this response spanned the rejected organ and peripheral blood, stimulated the differentiation of multiple B cell subsets, and produced a high-affinity, donor-specific, anti-HLA response. We found epitopic immunodominance that relied on highly exposed, solvent-accessible mismatched HLA residues as well as structural and biomolecular evidence of autoreactivity against the recipient's self-HLA allele. These alloreactive and autoreactive signatures converged in the recipient's circulating donor-specific Ab repertoire, suggesting that rejection requires both the recognition of non-self and breaches of tolerance to lead to alloinjury and graft loss.

INTRODUCTION

Antibodies (Abs) against mismatched human leukocyte antigens (HLA) are a leading cause of injury and graft loss in kidney transplantation.(Einecke et al., 2009; Gaston et al., 2010; Sellares et al., 2012) Up to 25% of kidney transplant recipients will develop a new donor-specific anti-HLA antibody (HLA-Ab) following transplant,(Everly et al., 2013) and these patients suffer a 40% absolute decline in 10-year graft survival.(Wiebe et al., 2012) The two arms of the humoral adaptive immune response, antibody-secreting cells (ASCs), which produce injurious donor-specific Abs, and memory B cells (Bmems), which augment alloresponses via antigen-presentation, cytokine elaboration,(Zeng et al., 2014) or differentiation into ASCs, work in concert to drive rejection. In addition to the above evidence indicating the importance of ASCs and their HLA-Abs, the detection of circulating alloreactive Bmems correlates with poor outcomes in transplantation.(Luque et al., 2019) Unfortunately, current therapies aimed at depleting ASCs and Bmems are largely ineffective, indicating the unmet need to both prevent and treat these alloresponses.(Schinstock et al., 2020)

This knowledge gap surrounding the immunology of B cell responses in transplant rejection largely exists because key features about the anatomy and specificity of the anti-HLA B cell response remain poorly understood. First, although ASCs that ultimately home to the bone marrow produce directly pathogenic donor-specific Abs,(Hill et al., 2023; Perry et al., 2008) it remains unknown whether the allograft, secondary lymphoid organs, or other sites host the immune response that generates alloreactive ASCs and Bmems. As different immune sites provide different methods of support to B cells,(Kwak et al., 2018; Lee et al., 2022; Liarski et al., 2014) this knowledge gap hinders the development of effective B cell-targeted immunosuppressive regimens. Second, although mismatched HLA residues are necessary to generate alloimmunity,(Merrill et al., 1956) the relative contributions and immunogenicity of these polymorphic residues remain unknown.(Bezstarosti et al., 2022; Honger et al., 2020; Tambur and Das, 2022) Without a structural understanding of HLA-specific B cell epitopes, the field lacks the ability to optimally match recipients and donors and protect patients from HLA-Ab formation, rejection, and graft loss.

In this manuscript, we evaluated the B cell alloimmune response in a single kidney transplant recipient with clinical features of anti-HLA donor-specific antibodies, antibody-mediated rejection (AMR), and ultimately, graft loss. We showed that B cells undergo clonal selection, differentiation, proliferation, and affinity maturation during organ rejection, that this response was enriched for donor-specific, alloreactive B cells, and that it spanned the rejected allograft and the peripheral blood. We deeply profiled the B cell response against a single mismatched donor HLA protein, revealing evidence of epitopic focusing and immunodominance. We solved the antibody/HLA structure of three anti-HLA Abs, revealing the structural basis of these HLA epitopes as well as the contribution of autoreactivity within the alloreactive B cell compartment. Finally, we show that this B cell response is clonally linked to circulating plasma anti-HLA Abs, tying together the two arms of the humoral alloimmune response. Ultimately, this work provides a framework for understanding the contribution of alloreactive B cells to transplant rejection and an epitopic basis for the discrimination of self from non-self.

RESULTS

The alloimmune response leads to transplant rejection and loss.
Prior work examining B cells in individuals with circulating donor specific antibodies (DSA) has shown that depletion of B cells using Rituximab(Moreso et al., 2018) or CD19-chimeric antigen receptor (CAR) T-cell therapy (Zhang et al., 2020) is largely ineffective in lowering levels of circulating DSA. These results support the hypothesis that long-lived ASCs are responsible for producing the DSA that contributes to allograft rejection and loss. However, the Bmem compartment represents another potential source of alloantibodies(Louis et al., 2021) and may mediate rejection independent of Ab production.(Zeng et al., 2014) The detection of alloreactive B cells is associated with poor outcomes (Luque et al., 2019; Wehmeier et al., 2019) and Bmems, particularly in tissues, are known to be ineffectively depleted by biologics like rituximab.(Mei et al., 2010) To test the potential contribution of Bmems to allograft rejection, we used blood and renal allograft samples from a single kidney transplant recipient, whose alloimmune responses culminated in antibody- and T cell-mediated rejection with subsequent graft loss. Serologically, we detected evidence of a robust anti-HLA ASC response, manifested by circulating IgG that was specific for the donor allograft – with clinically significant Ab responses against donor HLA class I and class II alleles, including A*01:01, A*32:01 and HLA DRB4*01:03. Histologically, this was manifested by the signs of macrovascular and microvascular injury consistent with antibody-mediated rejection (AMR). As the detection of circulating HLA-Abs by clinical assays suggested a significant donor-specific ASC response, we next looked to explore the contribution of alloreactive B cells to rejection and graft loss.

Intragraft and circulating B cells and antibody-secreting cells show features of antigen-driven selection.
Given the unanswered questions surrounding the B cell and anti-HLA Ab responses in organ transplant rejection, the fact that histopathology of this patient's allograft showed lymphocyte and ASC infiltration, we elected to study further the B cell response in this patient. Whether in secondary (Turner et al., 2020) or tertiary lymphoid structures (Chang et al., 2011), B cells undergo antigen-driven selection and clonal expansion and diversify their immunoglobulin gene receptors through T cell-dependent somatic hypermutation.(Liarski et al., 2014) To test whether the B cell compartment in the graft and peripheral blood showed features of antigen-driven selection, we obtained tissue from this patient's transplant nephrectomy specimen after his allograft was surgically removed as well as from his peripheral blood (Figure 1A). We sort-purified bulk populations of B cell subsets and ASCs from the processed kidney and blood and sequenced their variable heavy (V_H) chain (IgHV) genes by next-generation immunoglobulin sequencing. We analyzed clonal relationships within this dataset, assigning sequences to a clonal lineage if they shared V_H and joining (J_H) gene segments, identical heavy chain complementarity determining region (HCDR) lengths, and nucleotide identity >85% across the HCDR3.(Tipton et al., 2015) We defined an expanded lineage as any lineage without singletons that, when ranked by size, was at least 0.1% larger than the next smallest lineage.(Tipton et al., 2015) Immunoglobulin gene analysis revealed clonal expansion within the allograft, with rich connections between B cell subsets, including $CD27^+$ Bmems, IgD^-CD27^- double negative (DN) B cells, and $CD27^+CD38^+$ ASCs (Figure 1B). Compared to the blood and organ-specific B cell responses in nontransplant, brain dead organ donors, the allograft showed significantly more intra-tissue connections between subsets and inter-tissue connections between blood and kidney. To assess the degree of clonal diversity, we assessed the number of lineages that accounted for 20% (D_{20}) or 50% (D_{50}) of all sequences. In contrast to highly polyclonal repertoires in healthy control donors, these repertoires revealed oligoclonality in memory, DN, and ASC subsets. In addition, these responses revealed marked somatic hypermutation (SHM) across subsets, with similar degrees of SHM between Bmem and ASC subsets (Figure 1C) and class-switching with a preponderance of IgG isotype usage. Although most expanded lineages spanned both kidney and blood, several lineages were not identified in the blood, suggesting that some intragraft clonal expansions may not be detectable among circulating B cells.

Given these molecular signatures of expansion and clonal selection, we sought to evaluate the local immune environment of the allograft, specifically searching for microanatomic structures and phenotypic features that would support such a response. Previous work on B cell infiltrates in kidney transplant rejection has shown that specialized $CD4^+$ T cells within the germinal center, T follicular helper (T_{FH}) cells, formed conjugates with B cells in cases of mixed rejection (both AMR and T-cell mediated rejection [TCMR]), but not in cases of TCMR without AMR. However, even though conjugates were present in the AMR biopsies, the majority of intragraft B

cells were not associated with T_{FH} cells, suggesting the existence of at least two populations of intragraft B cells – those maintained by T_{FH} cells and those maintained through T_{FH}-independent mechanisms.(Liarski et al., 2014) Immunofluorescence of the allograft revealed clusters of proliferating B cells (Figure 1D) and ASCs (Figure 1E) within the allograft without evidence of well-organized TLOs as would be marked by T and B cell clusters or follicular dendritic cell networks.(Lee et al., 2022) Consistent with an ongoing extrafollicular response within the graft (and the apparent lack of germinal centers), our flow cytometry and sequencing data showed IgD^-CD27^- DN B cells that were similarly mutated to Bmems and ASCs. In addition, the cell surface phenotype of these intragraft DN B cells was chiefly $CD21^-CD11c^-$, similar to the DN3 extrafollicular response reported in severe cases of COVID-19.(Woodruff et al., 2020) Thus, the rejecting kidney hosted clonal expansion, proliferation, and differentiation of B cells as part of a robust adaptive immune response that spanned both kidney and peripheral blood.

Alloreactive B cells in the rejected graft and peripheral clonally expand, affinity mature, and display diverse patterns of reactivity targeting donor-specific HLA.

Prior work has identified B cell clonal expansion in kidney allografts with features of chronic injury (Cheng et al., 2011), and intragraft B cell infiltrates are known to correlate with poor outcomes.(Hippen et al., 2005; Tsai et al., 2006) However, the selecting antigens and mechanisms of B cell support remain largely undefined. For example, limited studies of human kidney transplants have suggested that intragraft B cells may be polyreactive (Ferdman et al., 2014; Porcheray et al., 2012) or autoreactive towards renal-specific or inflammation-specific autoantigens (Asano et al., 2021), while emerging murine data has shown that intragraft B cells may in fact be donor-specific for mismatched major histocompatibility complex (MHC) antigens.(Zhang et al., 2023) We hypothesized that allograft-infiltrating B cells would target mismatched HLA residues and display evidence of affinity maturation and clonal expansion. To test this hypothesis, we elected to study anti-HLA B cells that were specific for one of the mismatched donor HLA alleles – HLA A*01:01, and which corresponded to a significant levels of anti-A*01:01 donor-specific Abs in the patient's blood. We used fluorochrome-labeled tetramers of recombinant HLA A*01:01 to sort-purify single HLA-reactive B cells or ASCs from the allograft and the peripheral blood (Figure 2A). For these single cells, immunoglobulin (Ig) heavy and light chain genes were cloned, sequenced, and expressed as recombinant human IgG1. We profiled the fine specificity of recombinant monoclonal Abs (rmAbs) using HLA-coated microbeads and assessed biomolecular interactions using localized surface plasmon resonance (L-SPR).

Given the unique immune environment of the rejected allograft, we started our analysis with rmAbs generated from kidney-derived B cells. From the available nephrectomy tissue, we cloned a limited number of rmAbs, and three rmAbs were chosen for further analysis. We first confirmed that these rmAbs were A*01:01-specific against human cells, confirming binding against A*01:01-typed T cells. All rmAbs displayed nanomolar or subnanomolar affinities to A*01:01 by L-SPR, ranging from $1.9x10^{-9}$ M to $3.3x10^{-10}$ M. (Figure 2B). These three kidney-derived rmAbs were members of expanded lineages that spanned both kidney and blood populations. These three rmAbs were all derived from IgD^-CD27^+ Bmems based upon their index-sorting cell surface phenotype, but were connected to both ASCs and DN B cells in their expanded lineages. Immunogenetic analysis revealed these rmAbs were highly mutated with 19-32 V-region nucleotide mutations and nonsilent/silent mutation ratios suggesting antigen selection (range 1.46-3.33). After reverting these rmAbs to their unmutated common ancestors (UCAs), we found that all experienced total or near total abolition of A*01:01 reactivity, further supporting that these rmAbs affinity matured and that A*01:01 was the selecting antigen. Together, this indicates that that the rejected human renal allograft may host an alloreactive B cell response, and it indicates that these intragraft HLA-reactive B cells clonally expand and affinity mature against a donor-specific antigen.

As the alloimmune B cell response may also be detected occur outside of the rejecting graft,(Louis et al., 2021) we next studied the entire repertoire of the n=52 anti-A*01:01 reactive rmAbs we cloned and expressed, including those derived from peripheral blood B cells and those from the allograft. Within the peripheral blood, the A*01:01-reactive rmAbs were derived from a mix of Bmems, ASCs, and DN B cells. These anti-A*01:01 reactive rmAbs all displayed high affinity against A*01:01 (Figure 2C) and were also highly mutated, similar to the anti-A*01:01 rmAbs derived from the kidney. There were no significant differences in affinity or mutational burden based upon the cell-surface phenotype of either Bmem or ASC, running counter to the notion (Schinstock et al., 2020) that alloreactive B cells should be lower affinity, and possibly more cross-reactive,

than ASCs. To assess the fine specificity of these rmAbs, we determined their binding to 40 different HLA Class I alleles by cytometric bead array and normalized all MFIs as a percentage of the A*01:01 MFI, as that was the sorting antigen.

As an antigen's polymorphic residues may contribute to immune focusing and immunodominance (Lu et al., 2021) across B cell and ASC compartments,(Angeletti et al., 2017) we started by asking whether this anti-A*01:01, donor-specific rmAb response revealed evidence of immunodominance in its patterns of reactivity against various polymorphic residues. For these analyses, we combined all 49 blood derived and 3 kidney-derived rmAbs, clustering all 52 rmAbs based upon their patterns of HLA reactivity (Figure 2D). Given low amounts of HLA reactivity even after normalizing against negative control rmAbs, we defined HLA allelic reactivity as positive in the context of these pattern assignments if the rmAb bound a non-A*01:01 allele at a geometric mean fluorescence intensity (MFI) of at least 10% of the A*01:01 MFI, as A*01:01 was the sorting antigen. Sensitivity analyses performed using different percentage and absolute MFI values supported this threshold. This clustering revealed several major patterns of reactivity, and within our collection of 52 rmAbs, it revealed immunodominance of an A*01:01-monospecific pattern of reactivity. Given that there were seven polymorphic residues with at least 50 $Å^2$ of solvent-accessible surface area that differed between the donor's typing (A*01:01) and both of the recipient's HLA-A locus alleles (A*24:02 / A*30:01), we hypothesized that we would find 7 different patterns of reactivity, and that each pattern would receive $1/7^{th}$ (or 14.2%) of the B cell response. Compared to this null hypothesis, binomial testing revealed that the A*01:01 monospecific reactivity pattern (referred to subsequently as $A1^+$) was significantly immunodominant, with 19/52 (36.5%) rmAbs binding to A*01:01 alone (Fig 2E, $p<0.0001$). Within the monoclonal repertoire, a total of 8 expanded lineages contained rmAbs with an $A1^+$ monospecificity. The second most common pattern of reactivity, A*01:01+A*29:02+A*36:01+A*80:01, (referred to subsequently as $A1^+A29^+A36^+A80^+$) featured 5/52 (9.6%) rmAbs spread across 3 expanded lineages. In all, we identified 23 unique patterns of reactivity within this rmAb repertoire, far more than the seven hypothesized patterns based upon the seven mismatched residues between the donor's A*01:01 typing and the recipient's A*24:02/A*30:01 A-locus typing. Thus, although the donor-specific B cell response appears to target a diverse range of A*01:01-expressed epitopes, it also displays features of immunodominance, preferentially producing Abs that are monospecific to A*01:01. This suggests that although there may be multiple mismatched polymorphic residues between donor and recipient, certain residues, or epitopes, may be differentially immunogenic.

As an alternative to assessing immunodominance strictly within the monoclonal repertoire, we also investigated which patterns of reactivity were associated with the largest lineages from the bulk B cell receptor (BCR) dataset, spanning kidney and blood. Out of 6682 unique sequences in the bulk kidney and blood BCR datasets that could be clustered together with an A*01:01-reactive rmAb using the same V_H, J_H, HCDR3 length and >85% HCDR3 nucleotide identity, six distinct lineages each constituted at least 5% of all A*01:01-reactive sequences in the bulk BCR repertoire dataset. The JTK191A_K07 rmAb which was index-sorted with cell surface phenotype of ASC and was associated with 1289 ASC sequences in the blood, represented 25.5% of all A*01:01-linked bulk sequences. However, this monoclonal showed undetectable anti-A*01:01 binding by L-SPR (estimated KD > 1E-5M as compared to all other KDs <1E-6M) and had the lowest A*01:01 MFI among the 52 tested rmAbs. Given JTK191A_K07's exceedingly low anti-A*01:01 affinity, we chose to analyze other rmAbs with higher affinity towards the donor HLA. The next highest percentage of sequences was matched to Lin4, which had a $A1^+A29^+A36^+A80^+$ specificity similar to JTK191B_L02, a kidney-derived rmAb. Lin4 was linked to 636 kidney ASC sequences and Lin12, which also displayed $A1^+A29^+A36^+A80^+$ reactivity, was linked to 144 kidney ASCs (Figure 2F, depicting Lin4). In total, $A1^+A29^+A36^+A80^+$ rmAbs were linked to lineages constituting 24.2% of all bulk sequences. In addition to this $A1^+A29^+A36^+A80^+$ reactivity pattern, $A1^+$ monospecificity was heavily represented in the bulk BCR repertoire. $A1^+$ monospecific rmAbs were linked to 8 distinct lineages in the bulk dataset, comprising 2248 sequences (33.7% of the bulk dataset). Thus, two patterns of HLA reactivity dominated the bulk BCR repertoire, comprising 58.1% of all sequences. To better understand the epitopic and structural basis of these two immunodominant alloresponses, we solved two representative rmAb/HLA structures – JTK191B_E07, which demonstrated an $A1^+$ monospecific pattern of reactivity, and JTK191B_L02, which demonstrated an $A1^+A29^+A36^+A80^+$ pattern of reactivity.

The structural basis of alloreactivity

As we found evidence that certain patterns of reactivity were associated with significantly enhanced B cell responses, consistent with immunodominance, we sought to understand the structural basis of these B cell epitopes for two such responses. Although greater numbers of HLA residue mismatches between self and nonself are known to contribute to the formation of donor-specific anti-HLA Abs,(Senev et al., 2020) the immunogenicity of individual polymorphic residues is unknown. Thus, we next sought to understand the structural basis of alloreactivity and the interactions between the anti-HLA rmAb and the donor HLA. We hypothesized that the most solvent-accessible, most self-dissimilar polymorphic residues would drive immunodominant responses. We first selected a rmAb, JTK191B_E07 (subsequently referred to simply as "E07"), that targeted an immunodominant specificity and was part of an expanded lineage present in both kidney and blood (Figure 3A). The six rmAbs related to E07 within Lin2 demonstrated that same pattern of A*01:01-monospecificity. Using x-ray crystallography, we solved a 3.5Å structure of the E07 rmAb (expressed as a Fab) bound to HLA A*01:01 (Figure 3B). Both the Ab heavy and light chains made significant contacts with HLA epitope, binding to both monomorphic (identical between the donor A*01:01 protein and the recipient's self A*24:02/A*30:01 proteins) and polymorphic (mismatched between donor and at least one recipient allele) residues (Figure 3C). Contacts to residues that were double-mismatched, expressed on neither the recipient's A*24:02 or A*30:01 allele, included 156V and 163R (Figures 3D-E). These two residues, which are only expressed together on A*01:01 among the 40 HLA class I alleles tested for E07's reactivity, appear critical for this Fab's pattern of reactivity. Although these polymorphic residues appeared critical for the rmAb's specificity, overall, monomorphic self-residues dominated the surface area of the epitope. 864.3Å^2 of solvent-accessible surface area (SASA) was buried by E07 binding to A*01:01. Of this entire epitopic footprint, only 20.2% of the buried SASA (BSASA) came from residues that were double-mismatched (Figure 3D). 69.0% of the BSASA was contributed by residues that were monomorphic between donor and self-alleles. 10.8% of the BSASA was contributed by residues that were mismatched against only one of the self-alleles. The Fab formed hydrogen bonds with double-mismatched residues like 163R, monomorphic residues like 161E, and single-mismatched residues like 166D. Overall, the structure of E07 reveals that non-self-residues with large SASAs coordinate with extensive contacts to self-residues to produce a high-affinity, immunodominant specificity.

We then selected kidney-derived rmAb JTK191B_L02 (subsequently referred to as L02) which was part of an expanded lineage within both kidney and blood. This specific pattern of reactivity that was associated with L02's 787-member lineage (Lin12, Figure 4A), and was also associated with Lin4, an 827-member lineage (Figure 2F). L02 showed considerable connections to alloreactive Bmems, DNs, and ASCs spanning the rejected allograft and the blood (Figure 4A). Using CryoEM, we solved the structure of the L02 Fab binding A*01:01 to 3.2Å (Figure 4B). L02 buried a total area of 608.2Å^2 on the surface of A*01:01. Of this, only 9.7% of the BSASA came from double-mismatched residues. Similar to E07, 61.1% of the epitope's surface area derived from monomorphic residues matched to both self HLA alleles. L02 chiefly utilized HCDR3 and LCDR2 contacts with epitopic residues (Figure 4C); however, the light chain dominated the binding area of the interaction – contributing 69.6% of the paratope's BSASA. This corresponded to mutated LCDR2 and a LFR3 66S that formed a hydrogen-bond with the double-mismatched A*01:01 residue 76A (Figure 4D). The remainder of the light chain FR3 was draped over a 4-residue patch of single-mismatched residues (79G, 80T, 82R, 83G), forming multiple hydrogen bonds in this portion of the epitope (Figure 4E). The second double-mismatch in the epitope, 150V, was partially buried by the Fab's binding, but it formed no <5Å close contacts with heavy atoms in the Fab (Figure 4C). Also of note, 3 residues within the HLA's bound peptide were included in the epitope, one of which (6T) formed a hydrogen bond to a residue within the HCDR3, 113W. Review of a A*01:01-presented peptide atlas shows that T is the most frequent residue (9.6%) at residue six, although there is considerable diversity.(Marcu et al., 2021) Data showing that the L02 maintained consistent binding to A*01:01-typed T cells, which presumably present a variety of peptides, does not rule out the contribution of the peptide to L02's specificity, but suggests that it may be relatively minor. Thus, L02 differs from E07 by the extensive binding interactions provided by its light chain as well as more extensive peptide contacts. In addition, L02 utilizes considerably more hydrogen bonds, although only one is formed with a double-mismatched residue. Overall, the E07/A*01:01 and L02/A*01:01 structures reveal that while polymorphic residues may generate the fine specificity of an alloreactive Ab, there is a significant binding to self-residues both in terms of the buried area and the strength of the noncovalent interactions – even for Abs without measurable autoreactivity.

Convergence of alloreactivity and autoreactivity in the donor-specific alloresponse

Considering the significant contacts made by these alloreactive Abs against self-residues within the HLA epitope, we examined the repertoire of rmAbs for evidence of autoreactivity. To our surprise, we noted that almost 30% of rmAbs showed autoreactivity with evidence of anti-A*24:02 binding by cytometric bead array. Given the relatively high concentration of rmAbs used for the cytometric bead array assay, we first wanted to quantify the affinity of these Abs to both donor HLA (A*01:01) and the recipient self HLA (A*24:02), assessing the relative affinity of these A*01:01-reactive rmAbs to both donor and to self. Using L-SPR, we tested the anti-A*24:02 affinity of the rmAbs that had the highest A*24:02 MFIs by the cytometric bead array. We found that 20 (38% of all rmAbs) of these had measurable autoreactivity, with anti-A*24:02 KDs ranging from 1.2E-8M to 2.9E-6M (Figure 5A). For a subset of n=18 rmAbs with both anti-A*01:01 and anti-A*24:02 affinities measured by L-SPR, we noted a range in the relative affinities between two antigens, with some rmAbs showing affinity against the self-allele that ranged from 10-fold to 1000-fold weaker than the affinity against the donor allele.

As we noted that extensive contacts to monomorphic self-residues were present in the structures of E07/A*01:01 and L02/A*01:01, neither of which displayed measurable autoreactive binding to A*24:02, we then solved the structure of the JTK191B_M07 rmAb (hereafter referred to as M07), as this rmAb displayed measurable autoreactivity against A*24:02 and was part of an expanded lineage of rmAbs also displaying autoreactivity, Lin1 (Figures 5B-C). Similar to the earlier structures, this structure showed significant contacts with self-residues within the HLA epitope. However, unlike E07 and L02, M07's epitope only featured a single double-mismatched residue, 150V (Figures 5D-F). Although this residue 150V was partially buried by the Fab, it actually formed no <5Å close contacts with heavy atoms within the Fab. The remainder of epitope contained no double-mismatched residues (Figure 5G), and was identical to A*24:02, the self allele, with the exception of 127N (127K in the A*24:02 self-allele). 127N appears to support binding while the self-residue, 127K, might sterically hinder M07's binding to A*24:02, perhaps explaining the reduction in affinity to A*24:02 as compared to A*01:01. In addition, this 127N residue is the lone mismatched HLA residue which participates in a hydrogen bond. Thus, it appears that this 127N residue, which is a single-mismatch (A*24:02 features 127K), and not the 150V, which is double-mismatched, contributes to the almost a 1000-fold difference in M07's ability to discriminate between donor and self. Thus, the structure of M07 binding A*01:01 reveals the structural basis for its autoreactivity against A*24:02, revealing how peripheral, single-mismatched residues may tune the fine specificity and degree of autoreactivity within a given lineage.

Overlap of the autoreactive B cell compartment and the alloreactive plasma immunoglobulin repertoire

Although we had extensively detailed the B cell and ASC compartments, circulating donor-specific Abs are currently believed to be the most critical effectors of B cell-related allograft pathology. In order to assay the circulating HLA-Ab compartment, we performed plasma proteomics on the A*01:01-specific immunoglobulin (Ig) repertoire. We first affinity-purified circulating Ig from the kidney transplant recipient's plasma on an HLA-A*01:01 affinity column, revealing that the anti-A*01:01 response shows considerable cross-reactivity against other class I A-locus alleles but relatively few class I B-locus alleles (Figure 6A). We then compared the reactivity profile of the affinity-purified Abs (pAb) to the reactivity patterns of our n=52 rmAbs. Overall, the frequency of positive alleles as counted amongst the 52 rmAbs was strikingly similar to the MFI patterns of the pAb – showing the strongest reactivity towards A*01:01, A*36:01 and A*80:01 (Figure 6B). We then performed liquid chromatography tandem mass spectrometry (LC-MS/MS) on a tryptic digest of the pAb and the LC-MS/MS derived peptide sequences were used to probe an amino acid RepSeq database including all kidney, blood, and rmAb VDJ sequences. One example revealing peptides that closely matched an A*01:01-reactive lineage are shown (Figure 6C), with coverage from CDR1 into FR4. The plasma proteomics supports the phenotypic data of the lineage which shows a considerable number of ASCs, (Figure 6D) as well as the fact that C16 was surface-phenotyped as an ASC by index-sorting. In addition, this finding suggests that circulating autoreactive Abs may contribute to the alloreactive repertoire, as multiple rmAbs in Lin3 displayed measurable affinity to A*24:02, the recipient self-allele (Figure 6E). Overall, we found multiple examples of circulating Ig that shared extensive overlap with the B cells and ASCs detected within the graft – indicating that circulating donor-specific Ab responses may result from the convergence of alloreactive and autoreactive B cell responses.

DISCUSSION

Using a variety of molecular and structural approaches, we demonstrated that HLA-reactive B cells participated in organ transplant rejection by responding to donor-specific HLA. This response spanned the rejected organ and the peripheral blood, involved multiple B cell subsets, and promoted affinity-matured, immunodominant responses towards specific HLA epitopes. In addition to this vigorous recognition of non-self, we also showed this B cell response relied on extensive contacts with monomorphic, or self, HLA residues and that these self-residues may comprise over 90% of the HLA epitope. Consistent with these extensive interactions, over 40% of expressed rmAbs showed detectable binding to self HLA, demonstrating a breach of tolerance that coincides with the alloreactive response. Ultimately, we linked these monoclonal responses with the total B cell repertoire and with circulating Abs, showing the contribution of these principles to the Abs that drive transplant rejection.

Although donor-specific HLA-Abs and AMR driven by mismatched HLA proteins(Wiebe et al., 2013) remain a major cause of graft loss in kidney transplant recipients, the rules governing the immunogenicity of HLA mismatches are unknown.(Honger et al., 2020) In the context of antiviral responses, residue polymorphisms are known to contribute to immune focusing and immunodominance,(Lu et al., 2021) and thus we hypothesized that certain epitopic features would be critical in driving the alloimmune response against donor HLA. For two structures (E07/A*01:01 and L02/A*01:01), double-mismatched residues with considerable (>50$Å^2$) of solvent accessible surface area provide critical, specificity-determining contacts for the anti-HLA Ab. This suggests that certain mismatched residues are likely more immunogenic than others – and that if these immunogenic residues could be broadly identified, organ matching could be optimized to avoid highly immunogenic mismatches between donor and recipient pairs. The fact that anti-HLA patterns of reactivity of these two rmAbs could be linked to almost 60% of A*01:01-reactive B cell lineages suggests that understanding immunodominance and immunogenicity could translate to significant improvements in the magnitude of the alloimmune response and the likelihood of rejection.

Multiple studies have provided evidence for the development of autoreactivity in the context of solid organ transplantation, but these studies have focused on antigens to include tissue-specific, inflammatory, and endothelial antigens.(Asano et al., 2021; Clotet-Freixas et al., 2021; Saini et al., 2011) In contrast, we showed that autoreactivity can develop against self-HLA proteins, one of the most ubiquitously expressed and Ab-accessible proteins in the human body. Although certain autoimmune diseases are associated with a loss of central tolerance, marked by defects in light-chain receptor editing, this does not appear to be the case in this dataset. Almost all rmAbs which showed anti-A*24:02 autoreactivity displayed no or minimal detectable autoreactivity when reverted to an unmutated common ancestor. In addition, within a given lineage, anti-A*24:02 autoreactivity correlated strongly with anti-A*01:01 alloreactivity. This suggests that alloresponses, where T cell epitopes provide linked recognition via peptides that may not overlap with the B cell epitope, may present a specialized circumstance in which traditional peripheral tolerance mechanisms fail. Indeed, the amount of self-residue contacts within the HLA epitope suggests that in situations similar to the M07/A*01:01 structure, in which a single mismatched residue forms a close contact with the paratope, the immune system may be poised to facilitate the co-development of autoreactivity as the Ab affinity matures to an allo-epitope that is over 90% identical to the auto-epitope. Understanding how linked recognition succeeds and fails in both promoting immunity and censoring autoreactivity has implications in transplantation and multiple other contexts, including autoimmunity, vaccinology, and cancer immunotherapy. Finally, we speculate that autoreactive HLA-Abs may bind dually to self-HLA and donor-HLA. If the Abs have differential affinities, with a preference for donor HLA as shown in this study, the Abs may bind to the allograft and excess Abs may then bind to ubiquitously expressed self-HLA, rendering the DSA undetectable by traditional clinical assays. With the body serving as a sink, such a setting could produce the situation of DSA-negative AMR lesions. Indeed, this histology of AMR without detectable circulating DSA (Callemeyn et al., 2020) has been associated with the degree of HLA mismatch – suggesting an alloimmune mechanism even though none is detectable serologically.(Senev et al., 2022)

In conclusion, this work provides a framework for understanding the structural and molecular basis of B cell epitope targeting in organ transplant rejection. It highlights the anatomy of this alloresponse as it spans tissue and blood, producing a high-affinity donor specific response. Although non-self recognition may be critical for

certain immunodominant responses, self-recognition and a possible failure of linked recognition appear to conspire to generate autoreactivity within the alloreactive response. These findings suggest a path forward for understanding immunogenicity of donor HLA in the context of transplantation as well as the opportunity to use anti-HLA responses to better understand more fundamental questions of tolerance and immunity.

Limitations of the study

As this study was conducted with samples from a single patient, additional studies will be needed to assess the generalizability of these findings to other transplant patients, with different rejection pathologies involving a variety of HLA proteins, including HLA class II. The patient did have a history of systemic lupus erythematosus (SLE), which is associated with the production of anti-nuclear autoantibodies, but there is no definite evidence of auto-reactive anti-HLA Abs in patients with SLE. Given the vigorous alloresponse that was occurring and the lack of recurrent SLE nephritis by histopathology of the allograft, we speculate that the rejection against donor HLA was the dominant driver of disease pathology; however, we cannot exclude a possible role for SLE in our findings.

ACKNOWLEDGMENTS
We would like to acknowledge the NIH Tetramer Core facility for HLA-A*01:01 and HLA-A*24:02 tetramers, monomers, and expression plasmids. Sanger sequencing was conducted at the Genetic Resources Core Facility (RRID SCR_018669) at Johns Hopkins University Department of Genetic Medicine, Baltimore, MD as well as at the Heflin Sequencing Core at the University of Alabama at Birmingham Heersink School of Medicine. We thank Vidyasagar Hanumanthu, director of the UAB Flow Core Facility, and Dr. Michael Crowley, director of the UAB Heflin Genomics core for their assistance with these studies. We also thank Dr. Daryl Good and Dr. Susan Kelso of Nicoya for their assistance in the conduct and analysis of localized surface plasmon resonance experiments. Research reported in this manuscript was supported by grants from the National Institutes of Health: NIDDK T32 DK007545 to J.T.K., NIAID T32 AI007051 to J.T.K., and NIAID U19 AI142737 to F.E.L. The content is solely the responsibility of the authors and does not necessarily represent the official views of the National Institutes of Health.

AUTHOR CONTRIBUTIONS
F.E.L. and J.T.K. conceived the study. F.E.L. secured funding, oversaw project administration, participated in the original drafting of the manuscript and its revisions, and provided direct supervision. J.T.K. conducted experiments, performed formal analyses, curated data, visualized data, wrote the original draft of the manuscript and participated in its revisions. R.G.K. conducted experiments, provided methodologic expertise, validated key reagents, conducted formal analyses, curated data, assisted with proteomic visualization, and provided supervision. T.J.G. provided methodologic expertise, conducted experiments and formal analyses, curated data, and provided supervision. J.L.K conducted formal analyses of structural data. C.F.F. provided methodologic expertise, conducted formal analyses, and generated visualizations of repertoire data. A.F.R provided methodologic expertise and supervision. R.D.A, S.Q., A.S.S., and B.J.M. conducted experiments. K.J.M., A.R.C., G.Y., M.E.H., and J.A. provided key reagents. S.C.O., V.K., J.A.H., and F.D.R assisted with formal analysis of the clinical record. J.F.K. and T.D.R supervised and facilitated project administration. E.O.S supervised, facilitated project administration, and provided critical resources. P.M.P. reviewed and edited the manuscript. J.A.M. provided methodologic expertise, software, and conducted formal analyses.

DECLARATION OF INTERESTS
The authors have no conflicts of interest to declare.

MAIN FIGURE LEGENDS

Figure 1. The B cell response in organ transplant rejection.
(A) Schematic outlining sample acquisition and major experiments. After tissue processing, B cells and antibody-secreting cells (ASCs) from a rejected transplanted kidney and the peripheral blood of that same patient were sort-purified for bulk B-cell receptor VDJ sequencing and generation of single HLA-reactive recombinant monoclonal antibodies (Abs). **(B)** Alluvial plots depicting the connections between expanded lineages of B cell subsets within the kidney (120,000 cells) and blood (6,824 cells) of the patient with kidney transplant rejection. B cell lineages are defined as having an identical V_H and J_H gene segment annotation, identical HCDR3 length, and HCDR3 nucleotide sequence identity of >85%. Shared lineages, identified between blood and tissue B cell subsets are represented as alluvial plots with individual lineages ranked by size in each subset. Numbers below columns reflect cells sorted for VDJ sequencing, unique lineages, and lineages with greater than one sequence assigned. D50 refers to sequences positioned in the top 50% of a given subset's distribution. Cell surface phenotypes were: ASC ($CD27^+CD38^+$), DN (IgD^-CD27^-) and MEM (nonASC, $CD27^+$) **(C)** V-region nucleotide (NT) mutation frequency across sort and technical replicates of B cell subsets from the rejected kidney, reflecting bimodal distribution with a range of NT mutations from 5-20 for most cells. **(D-E)** Immunofluorescent histochemistry of the rejected kidney shows clusters of proliferating B cells ($CD19^+Ki\text{-}67^+$) and ASCs ($CD19^+IgH^+CD38^+$).

Figure 2. The B cell response to mismatched donor HLA reveals affinity maturation, clonal expansion, and epitopic focusing.
(A) Cells from the transplant nephrectomy specimen and peripheral blood mononuclear cells were stained with fluorescently labeled recombinant HLA tetramer matching the organ transplant donor allele of HLA-A*01:01. Live $CD19^+$ non-naïve (not IgD^+CD27^-) cells that stained double positive with the A*01:01 tetramers were index-sorted for single cell recombinant monoclonal antibody (rmAb) production. **(B)** Three rmAbs derived from kidney memory B cells were studied for binding to HLA-A*01:01. Binding kinetics are shown, fit as 1:1 Langmuir curves against biotinylated A*01:01 by localized surface plasmon resonance (L-SPR). **(C)** A plot showing the anti-A*01:01 affinity of all expressed rmAbs. Following kinetic fitting for all rmAbs, anti-A*01:01 equilibrium constants were calculated (KD). Based upon the maximum tested concentration of each rmAb, 1.3uM, a limit of detection for the weakest KD of 1E-5M was inferred. **(D)** n=52 rmAbs were incubated with 40 different HLA-coated microbeads and stained with an anti-IgG secondary antibody. Geometric mean fluorescence intensities (MFIs) were normalized against a panel of negative (flu-specific) control human rmAbs. Normalized MFIs were log transformed and clustered using Euclidean distance as the similarity measure. All antibodies show anti-A*01:01 binding above the negative threshold value of the assay, and a variety of reactivity patterns with other HLA Class I alleles. **(E)** rmAb reactivity patterns were further clustered by converting normalized MFIs into binary variables (positive/negative) if the normalized MFI for the antigen was at least 10% of the A*01:01 normalized MFI. Following this transformation, rmAbs were then grouped by patterns of reactivity, testing a null hypothesis that there would be 7 different patterns of reactivity corresponding to the 7 mismatched amino acid residues expressed on the donor A*01:01 as compared to the recipient's HLA typing. Compared to this null hypothesis, an A*01:01 monospecific pattern of reactivity was observed significantly more often than expected (36.5% vs. 14.3%, $p<0.0001$). **(F)** Expanded lineage of B cells depicted using a phylogenetic tree, constructed using Phylip's DNA parsimony tool, with nodes indicating cell surface phenotype and edges tracing mutations away from an unmutated common ancestor (black node) through inferred mutations (gray nodes) for Lin4, for which related rmAbs displayed an A*01:01 monospecific pattern of reactivity consistent with the immunodominant pattern found in **(E)**. Data were analyzed using a binomial test and the confidence interval of the proportion was calculated using the hybrid Wilson/Brown method **(E)**.

Figure 3. The structural basis of E07/A*01:01 alloimmune recognition.
(A) Lin2, an expanded lineage of B cells containing the E07 rmAb, depicted using a phylogenetic tree, constructed using Phylip's DNA parsimony tool, with nodes indicating cell surface phenotype and edges tracing mutations away from an unmutated common ancestor (black node) through inferred mutations (gray nodes). **(B)** The E07 rmAb was engineered and expressed as a Fab and complexed with donor HLA-A*01:01. The structure of the complex was determined using X-ray crystallography. HLA-A*01:01 alpha chain is shown in coral, beta-2-microglobulin in dark khaki, and peptide in slate gray. The E07 light chain is shown in dodger blue

and the heavy chain is shown in dark red. The epitope is colored with monomorphic (identical to self-HLA) residues in black and double-mismatched residues in firebrick red. **(C)** Circos plot depicting close (<5Å interatomic distance between non-hydrogen Fab atom and HLA-A*01:01 alpha chain atom) contacts. The numbering outside each segment indicates the residue number for the given chains: A*01:01, E07 heavy chain, and E07 light chain. The outer ring of the A*01:01 alpha chain shows the solvent accessible surface area of the residue in the unbound form of HLA-A*01:01. The outer ring of the Ab segments indicates the IMGT region of the residue, either framework (FR) or complementarity-determining (CDR). The inner ring of the A*01:01 alpha chain segment indicates whether the residue is monomorphic or polymorphic. The inner ring of the Ab segments indicates whether the residue is mutated from the germline reference allele. Links depict hydrogen bonds (red) and <5Å close contacts. **(D)** Depicts an alternate angle of the E07 epitope in black on HLA-A*01:01, with double-mismatched residues in firebrick red. **(E)** A heatmap depicting the features of the 21 epitopic residues bound by E07. HLA-A*01:01 residues are numbered at the top of the heatmap. The first row indicates the amount of solvent-accessible area that is buried by the Fab's binding. The second row indicates the type of residue mismatch, as compared to the recipient's self-alleles. The third row indicates the Ellipro score of the residue in the HLA-A*01:01 unbound form. And the final row indicates whether the residue participates in a hydrogen bond with the Fab.

Figure 4. The structural basis of L02/A*01:01 alloimmune recognition.
(A) Lin12, an expanded lineage of B cells containing the L02 rmAb, depicted using a phylogenetic tree, constructed using Phylip's DNA parsimony tool, with nodes indicating cell surface phenotype and edges tracing mutations away from an unmutated common ancestor (black node) through inferred mutations (gray nodes). **(B)** The L02 rmAb was engineered and expressed as a Fab and complexed with donor HLA-A*01:01. The structure of the complex was determined using cryogenic electron microscopy. HLA-A*01:01 alpha chain is shown in coral, beta-2-microglobulin in dark khaki, and peptide in slate gray. The L02 light chain is shown in plum and the heavy chain is shown in purple. The epitope is colored with monomorphic (identical to self-HLA) residues in black and double-mismatched residues in firebrick red. **(C)** Circos plot depicting close (<5Å interatomic distance between non-hydrogen Fab atom and HLA-A*01:01 alpha chain atom) contacts. The numbering outside each segment indicates the residue number for the given chains: A*01:01, L02 heavy chain, and L02 light chain. The outer ring of the A*01:01 alpha chain shows the solvent accessible surface area of the residue in the unbound form of HLA-A*01:01. The outer ring of the Ab segments indicates the IMGT region of the residue, either framework (FR) or complementarity-determining (CDR). The inner ring of the A*01:01 alpha chain segment indicates whether the residue is monomorphic or polymorphic. The inner ring of the Ab segments indicates whether the residue is mutated from the germline reference allele. Links depict hydrogen bonds (red) and <5Å close contacts. **(D)** Depicts an alternate angle of the L02 epitope in black on HLA-A*01:01, with double-mismatched residues in firebrick red. **(E)** A heatmap depicting the features of the 20 epitopic residues bound by L02. HLA-A*01:01 residues are numbered at the top of the heatmap. The first row indicates the amount of solvent-accessible area that is buried by the Fab's binding. The second row indicates the type of residue mismatch, as compared to the recipient's self-alleles. The third row indicates the Ellipro score of the residue in the HLA-A*01:01 unbound form. And the final row indicates whether the residue participates in a hydrogen bond with the Fab.

Figure 5. Anti-HLA autoreactivity and alloreactivity converge in transplant rejection.
(A) A plot showing the anti-A*01:01 (alloreactive) and anti-A*24:02 (autoreactive) affinity of n=18 rmAbs with detectable anti-A*24:02 reactivity by cytometric bead array. Following kinetic fitting for all rmAbs, anti-HLA equilibrium constants were calculated (KD). Based upon the maximum tested concentration of each rmAb, 1.3uM, a limit of detection for the weakest KD of 1E-5M was inferred. **(B)** Lin1, an expanded lineage of autoreactive B cells containing the M07 rmAb, depicted using a phylogenetic tree, constructed using Phylip's DNA parsimony tool, with nodes indicating cell surface phenotype and edges tracing mutations away from an unmutated common ancestor (black node) through inferred mutations (gray nodes). **(C)** A plot showing the anti-A*01:01 (alloreactive) and anti-A*24:02 (autoreactive) affinity of all 10 rmAbs in Lin1. Following kinetic fitting for all rmAbs, anti-HLA equilibrium constants were calculated (KD). Based upon the maximum tested concentration of each rmAb, 1.3uM, a limit of detection for the weakest KD of 1E-5M was inferred. There was a strong (r=0.802) and significant (p=0.007) association between the autoreactive and alloreactive affinity of each rmAb. **(D)** The M07 rmAb was engineered and expressed as a Fab and complexed with donor HLA-A*01:01. The structure of the complex was determined using cryogenic electron microscopy. HLA-A*01:01

alpha chain is shown in coral, beta-2-microglobulin in dark khaki, and peptide in slate gray. The M07 light chain is shown in goldenrod and the heavy chain is shown in dark olive green. The epitope is colored with monomorphic (identical to self-HLA) residues in black and double-mismatched residues in firebrick red. **(E)** Circos plot depicting close (<5Å interatomic distance between non-hydrogen Fab atom and HLA-A*01:01 alpha chain atom) contacts. The numbering outside each segment indicates the residue number for the given chains: A*01:01, M07 heavy chain, and M07 light chain. The outer ring of the A*01:01 alpha chain shows the solvent accessible surface area of the residue in the unbound form of HLA-A*01:01. The outer ring of the Ab segments indicates the IMGT region of the residue, either framework (FR) or complementarity-determining (CDR). The inner ring of the A*01:01 alpha chain segment indicates whether the residue is monomorphic or polymorphic. The inner ring of the Ab segments indicates whether the residue is mutated from the germline reference allele. Links depict hydrogen bonds (red) and <5Å close contacts. **(F)** Depicts an alternate angle of the M07 epitope in black on HLA-A*01:01, with double-mismatched residues in firebrick red. **(G)** A heatmap depicting the features of the 22 epitopic residues bound by M07. HLA-A*01:01 residues are numbered at the top of the heatmap. The first row indicates the amount of solvent-accessible area that is buried by the Fab's binding. The second row indicates the type of residue mismatch, as compared to the recipient's self-alleles. The third row indicates the Ellipro score of the residue in the HLA-A*01:01 unbound form. And the final row indicates whether the residue participates in a hydrogen bond with the Fab. Data were analyzed using a nonparametric Spearman correlation with a two-tailed P value **(C)**.

Figure 6. Plasma proteomics links circulating immunoglobulins to donor-specific and autoreactive B cell lineages.
(A) Heatmap depicting the anti-HLA reactivity patterns of the recipient's plasma and A*01:01-specific circulating antibody repertoire. The transplant recipient's plasma (diluted from 1620-fold to 320,000-fold) and A*01:01-specific immunoglobulins (Ig) from plasma that had been affinity purified using an HLA-A*01:01 affinity column (diluted from 5000 ng/mL to 2 ng/mL) were incubated with HLA-coated microbeads, stained with an anti-IgG fluorescent secondary, and anti-HLA geometric mean fluorescence intensity (MFI) values were determined via flow cytometry. MFI 1000 was set as a negative threshold, and MFI values were log10 transformed. **(B)** Plot comparing the monoclonal repertoire of HLA reactivities to the A*01:01-specific circulating antibody repertoire. The upper plot shows the number of HLA Class I alleles bound by the n=52 rmAbs, where a positive allele is one whose MFI is at least 10% of the A*01:01 MFI for a given rmAb. The bottom plot shows the same MFI dilution data that is depicted in **(A)** for the A*01:01-affinity purified Ig. **(C)** Liquid chromatography tandem mass spectrometry (LC-MS/MS) analysis of a tryptic digest of the A*01:01-affinity purified plasma Ig. The MS-derived peptide amino acid (aa) sequences were used to probe a RepSeq database including all BCR sequences derived from the kidney, blood and rmAb rep-seq libraries (13,466 lineages with >1 one sequence) and an unrelated large RepSeq dataset (323,000 lineages). Exact peptide matches to lineage sequences were determined and members of the lineages were ranked by % aa matched of total. Peptide sequences are plotted by position within VDJ sequence and colored by the frequency of matches across the data set. 68% of the C16 heavy chain VDJ was identified, including two peptide sequence spanning CDR regions that are rare within the sequence database. **(D)** Lin3, an expanded lineage of alloreactive and autoreactive B cells containing the C16 rmAb from panel **(C)**, depicted using a phylogenetic tree, constructed using Phylip's DNA parsimony tool, with nodes indicating cell surface phenotype and edges tracing mutations away from an unmutated common ancestor (black node) through inferred mutations (gray nodes). **(E)** A plot showing the anti-A*01:01 (alloreactive) and anti-A*24:02 (autoreactive) affinity of n=3 tested rmAbs within Lin3. Following kinetic fitting for all rmAbs, anti-HLA equilibrium constants were calculated (KD). Based upon the maximum tested concentration of each rmAb, 1.3uM, a limit of detection for the weakest KD of 1E-5M was inferred.

Figure 1.

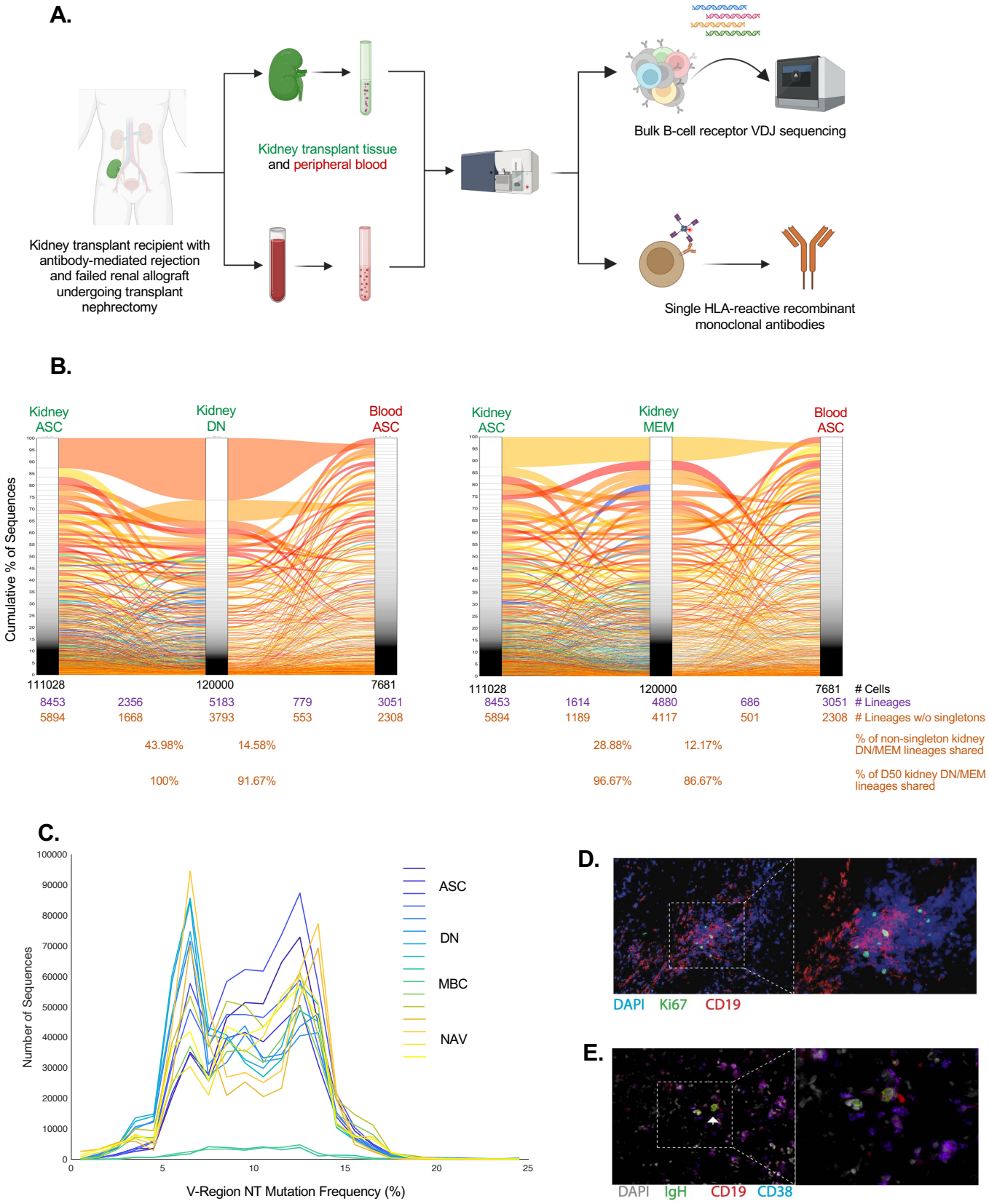
A.
Kidney transplant tissue
and peripheral blood
Kidney transplant recipient with antibody-mediated rejection and failed renal allograft undergoing transplant nephrectomy
Bulk B-cell receptor VDJ sequencing
Single HLA-reactive recombinant monoclonal antibodies
B.
Kidney ASC
Kidney DN
Blood ASC
Kidney ASC
Kidney MEM
Blood ASC
Cumulative % of Sequences
111028
120000
7681
111028
120000
7681
Cells
8453 2356 5183 779 3051
8453 1614 4880 686 3051
Lineages
5894 1668 3793 553 2308
5894 1189 4117 501 2308
Lineages w/o singletons
43.98% 14.58%
28.88% 12.17%
% of non-singleton kidney DN/MEM lineages shared
100% 91.67%
96.67% 86.67%
% of D50 kidney DN/MEM lineages shared
C.
Number of Sequences
V-Region NT Mutation Frequency (%)
ASC
DN
MBC
NAV
D.
DAPI Ki67 CD19
E.
DAPI IgH CD19 CD38

Figure 2.

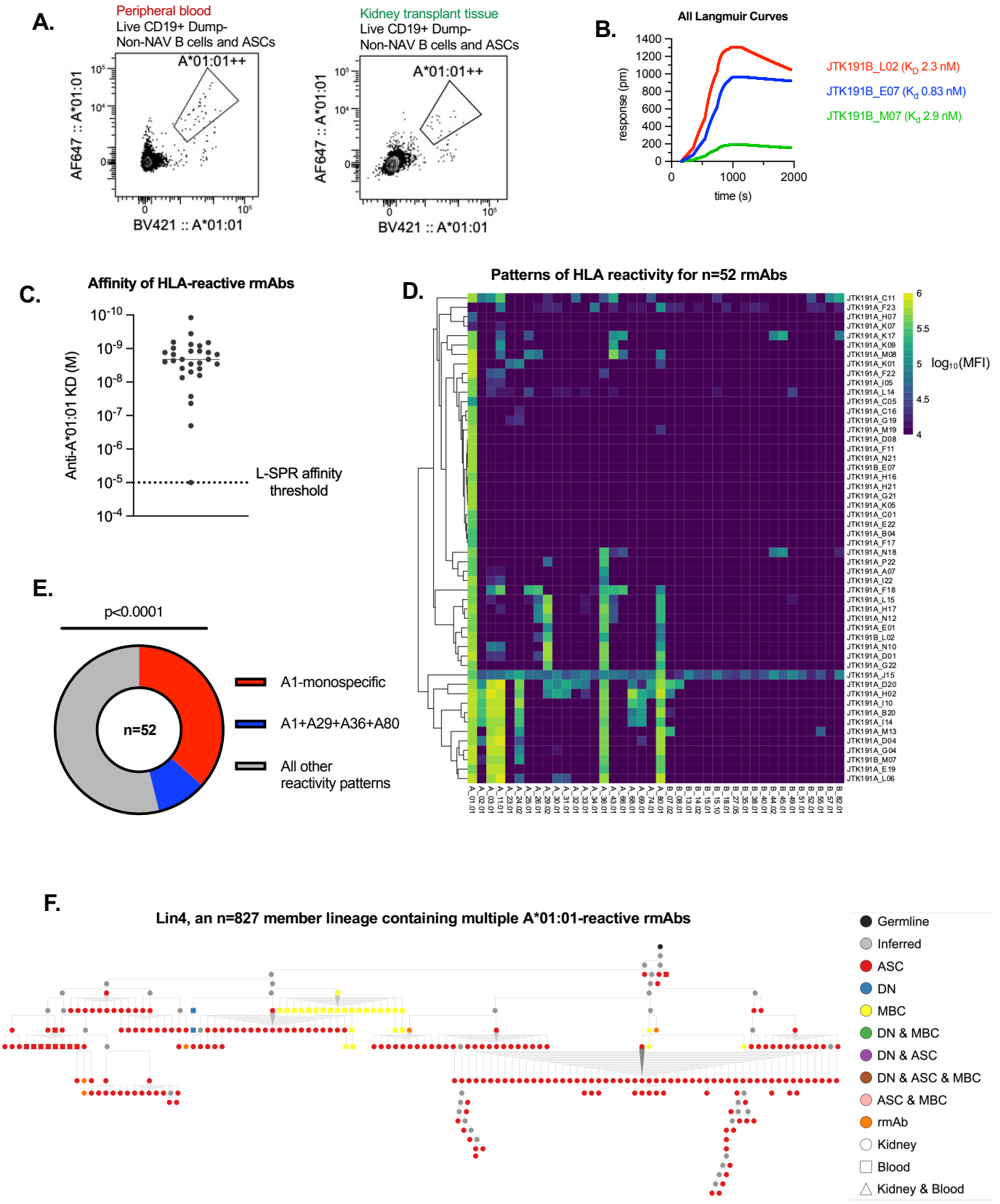
A.
Peripheral blood
Live CD19+ Dump-
Non-NAV B cells and ASCs
A*01:01++
AF647 :: A*01:01
BV421 :: A*01:01
Kidney transplant tissue
Live CD19+ Dump-
Non-NAV B cells and ASCs
A*01:01++
AF647 :: A*01:01
BV421 :: A*01:01
B.
All Langmuir Curves
response (pm)
time (s)
JTK191B_L02 (K_D 2.3 nM)
JTK191B_E07 (K_d 0.83 nM)
JTK191B_M07 (K_d 2.9 nM)
C.
Affinity of HLA-reactive rmAbs
Anti-A*01:01 KD (M)
L-SPR affinity threshold
D.
Patterns of HLA reactivity for n=52 rmAbs
log10(MFI)
E.
p<0.0001
n=52
A1-monospecific
A1+A29+A36+A80
All other reactivity patterns
F.
Lin4, an n=827 member lineage containing multiple A*01:01-reactive rmAbs
Germline
Inferred
ASC
DN
MBC
DN & MBC
DN & ASC
DN & ASC & MBC
ASC & MBC
rmAb
Kidney
Blood
Kidney & Blood

Figure 3.

A.

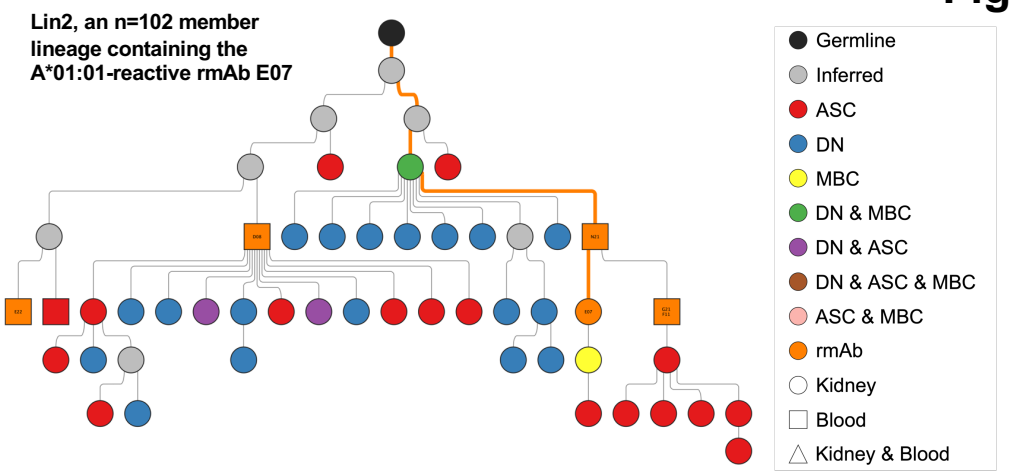

B.

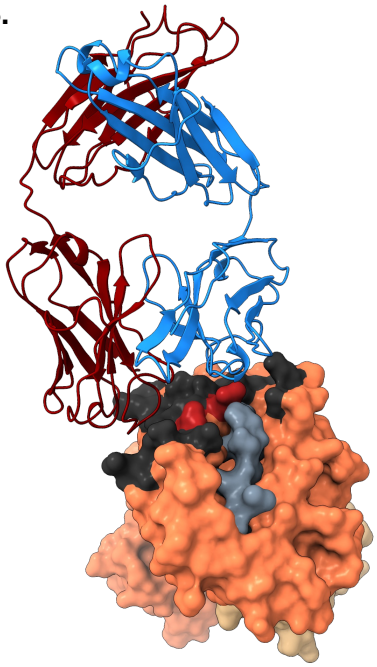

C.

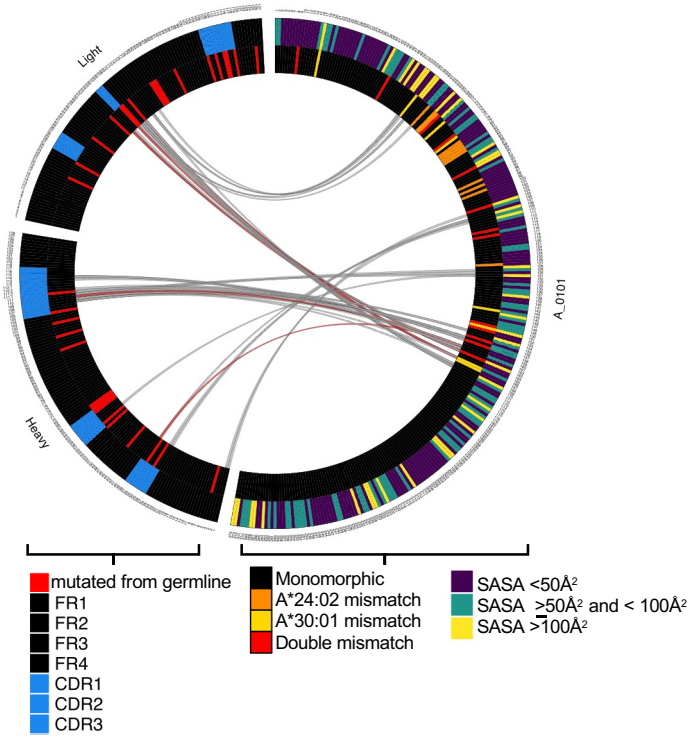

D.

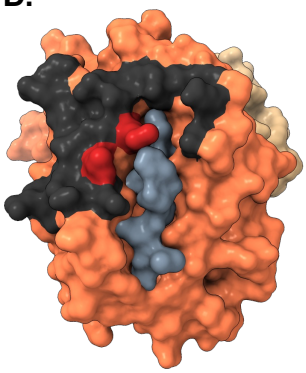

E.

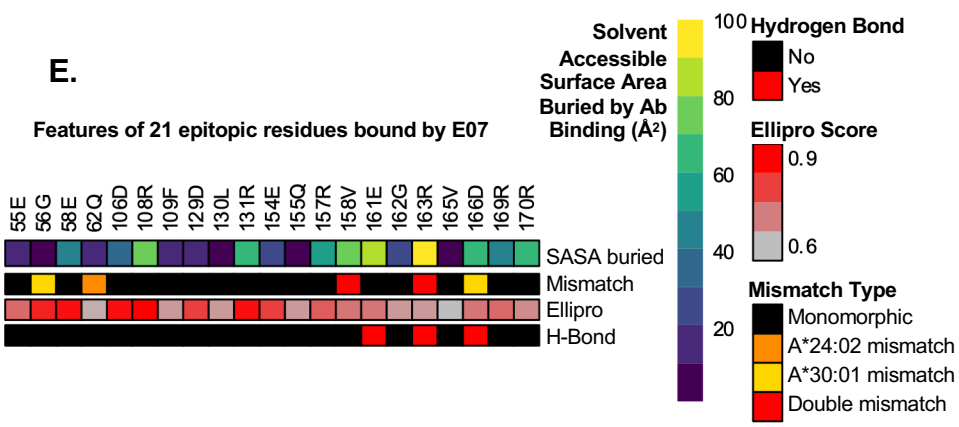

Figure 4.

A.

Lin12, an n=787 member lineage containing the A*01:01-reactive rmAb L02

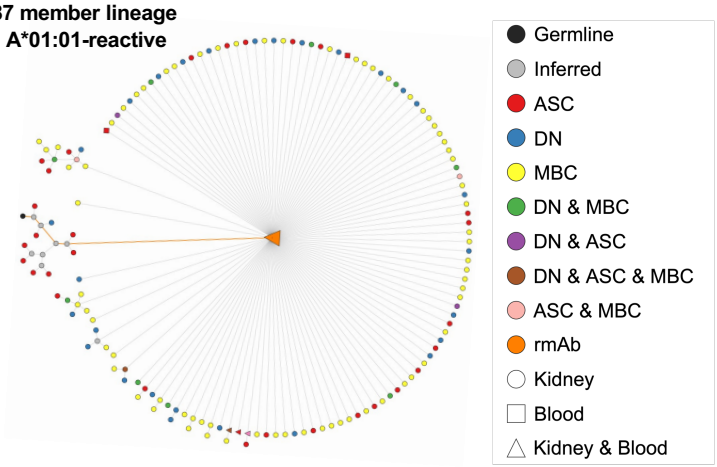

B.

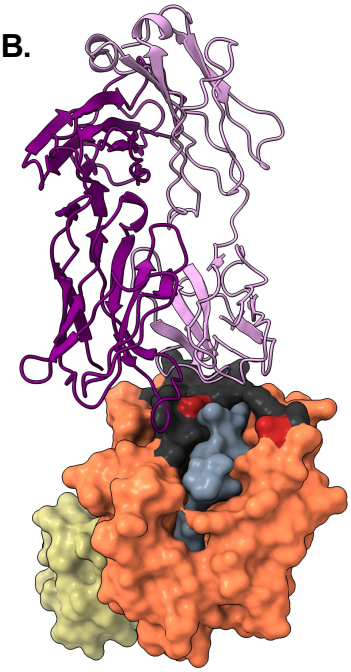

C.

Close contacts between L02 Heavy Chain and Light Chain with A*01:01

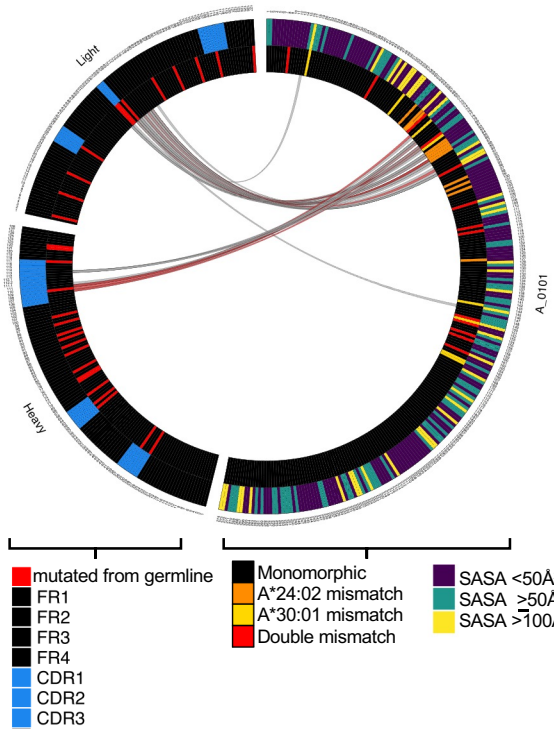

F.

D.

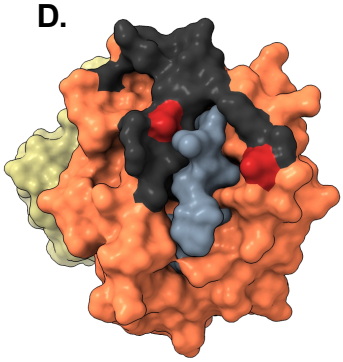

E.

Features of 20 epitopic residues bound by L02

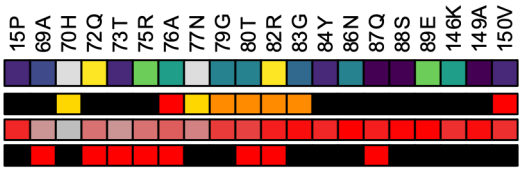

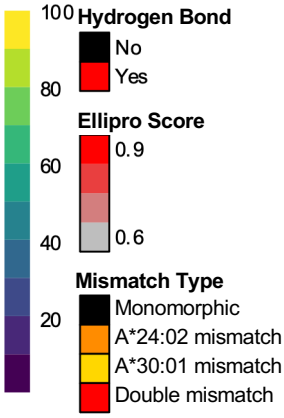

Figure 5.

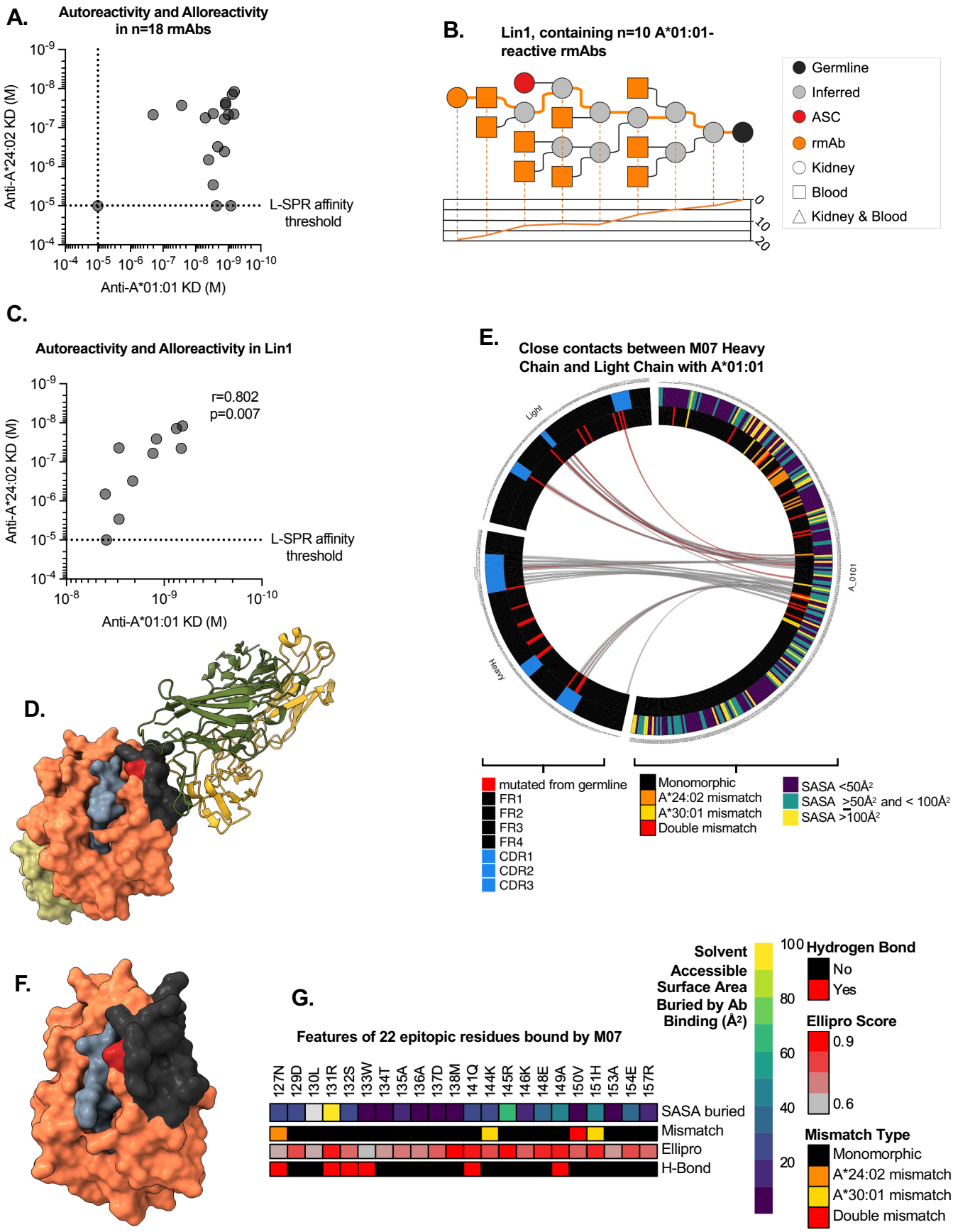
A.
Autoreactivity and Alloreactivity in n=18 rmAbs
Anti-A*24:02 KD (M)
Anti-A*01:01 KD (M)
L-SPR affinity threshold
B.
Lin1, containing n=10 A*01:01-reactive rmAbs
Germline
Inferred
ASC
rmAb
Kidney
Blood
Kidney & Blood
C.
Autoreactivity and Alloreactivity in Lin1
r=0.802
p=0.007
Anti-A*24:02 KD (M)
Anti-A*01:01 KD (M)
L-SPR affinity threshold
D.
E.
Close contacts between M07 Heavy Chain and Light Chain with A*01:01
Light
Heavy
A_0101
mutated from germline
FR1
FR2
FR3
FR4
CDR1
CDR2
CDR3
Monomorphic
A*24:02 mismatch
A*30:01 mismatch
Double mismatch
SASA <50Å²
SASA ≥50Å² and < 100Å²
SASA ≥100Å²
F.
G.
Features of 22 epitopic residues bound by M07
127N 129D 130L 131R 132S 133W 134T 135A 136A 137D 138M 141Q 144K 145R 146K 148E 149A 150V 151H 153A 154E 157R
SASA buried
Mismatch
Ellipro
H-Bond
Solvent Accessible Surface Area Buried by Ab Binding (Å²)
100
80
60
40
20
Hydrogen Bond
No
Yes
Ellipro Score
0.9
0.6
Mismatch Type
Monomorphic
A*24:02 mismatch
A*30:01 mismatch
Double mismatch

Figure 6.

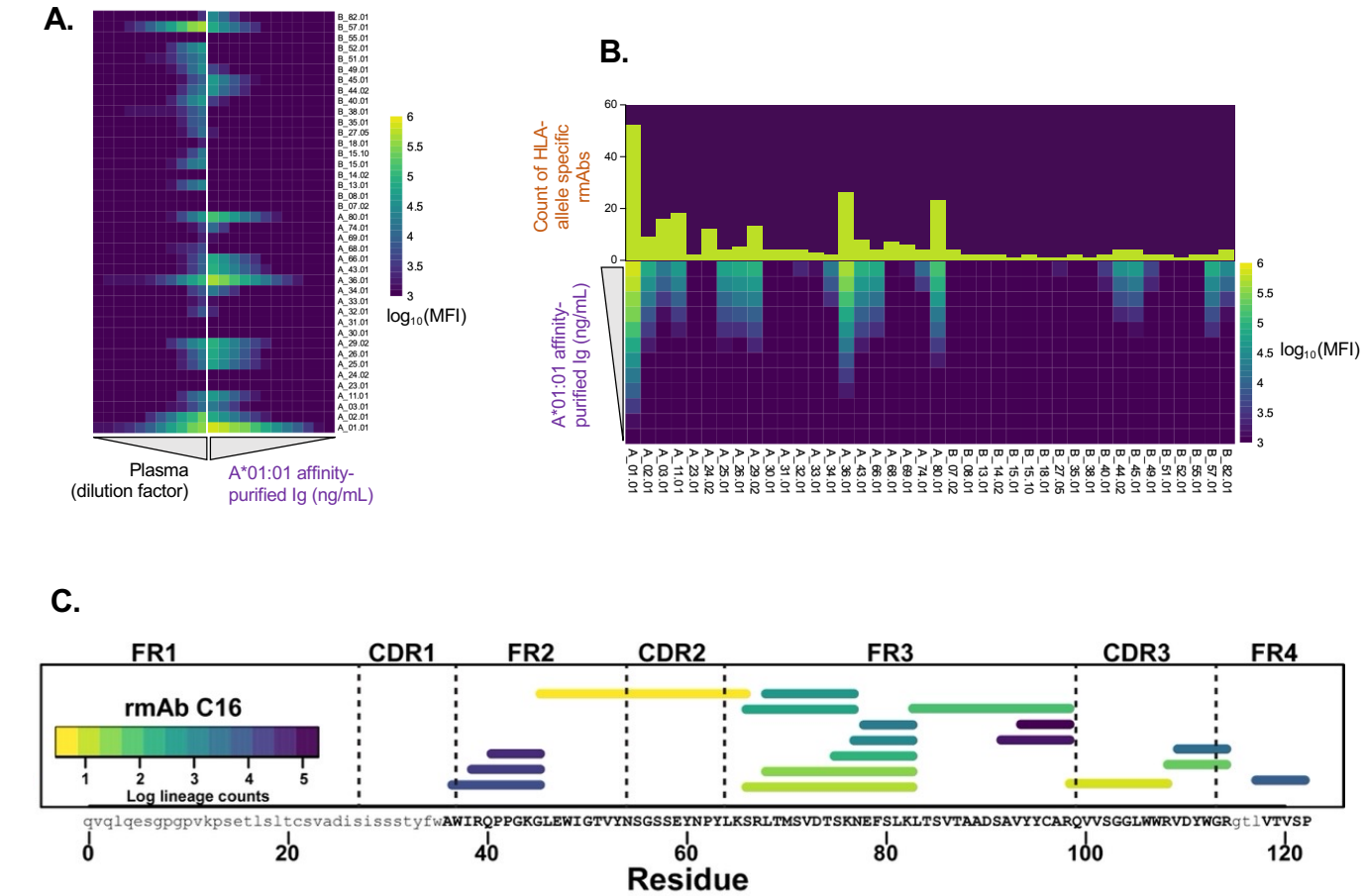
A.
Plasma
(dilution factor)
A*01:01 affinity-
purified Ig (ng/mL)
log10(MFI)
B.
Count of HLA-
allele specific
rmAbs
A*01:01 affinity-
purified Ig (ng/mL)
log10(MFI)
C.
FR1
CDR1
FR2
CDR2
FR3
CDR3
FR4
rmAb C16
Log lineage counts
qvqlqesgpgpvkpsetlsltcsvadisissstyfwAWIRQPPGKGLEWIGTVYNSGSSEYNPYLKSRLTMSVDTSKNEFSLKLTSVTAADSAVYYCARQVVSGGLWWRVDYWGRgtlVTVSP
Residue

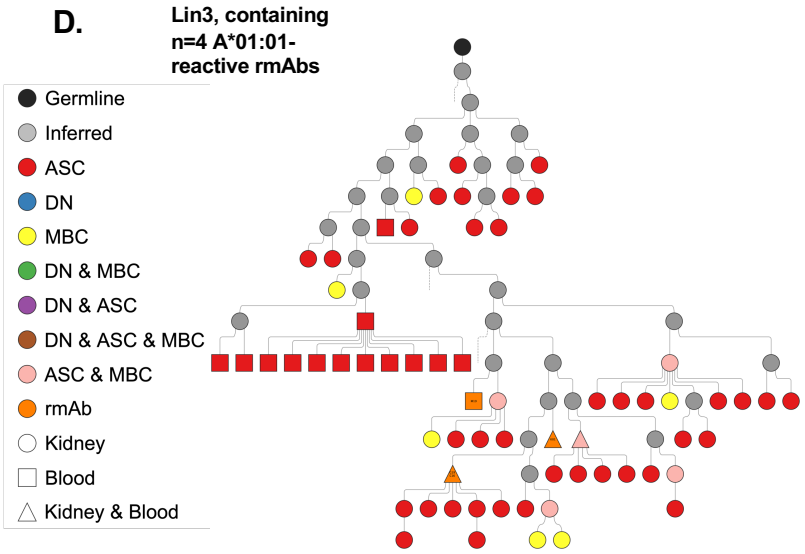
D.
Lin3, containing
n=4 A*01:01-
reactive rmAbs
Germline
Inferred
ASC
DN
MBC
DN & MBC
DN & ASC
DN & ASC & MBC
ASC & MBC
rmAb
Kidney
Blood
Kidney & Blood

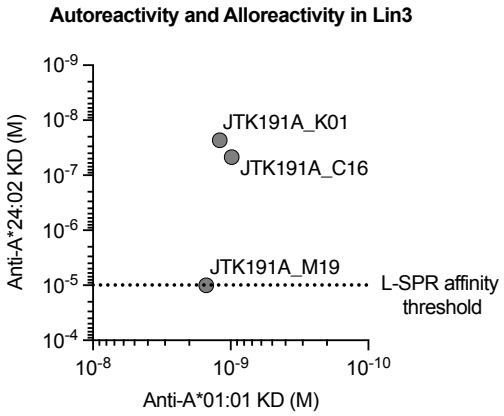
E.
Autoreactivity and Alloreactivity in Lin3
JTK191A_K01
JTK191A_C16
JTK191A_M19
L-SPR affinity
threshold
Anti-A*24:02 KD (M)
Anti-A*01:01 KD (M)

Table 1. Data collection and refinement statistics of crystal structure of E07/HLA-A*01:01 complex.

Wavelength (Å)	1.000
Resolution range (Å)	30.13 - 3.84 (3.977 - 3.84)
Space group	C 1 2 1
Unit cell	357.07 259.58 255.36 90 133.13 90
Total reflections	586637
Unique reflections	154424 (11218)
Multiplicity	3.776
Completeness (%)	95.60 (69.98)
Mean I/sigma(I)	8.05 (1.77)
Wilson B-factor	103.72
R-merge	0.172 (0.597)
R-meas	0.199 (0.699)
R-pim	0.100 (0.360)
CC1/2	0.981 (0.710)
CC*	0.995 (0.911)
Reflections used in refinement	154387 (11215)
Reflections used for R-free	2017 (145)
R-work	0.2199
R-free	0.2661
Number of non-hydrogen atoms	66391
macromolecules	66391
ligands	0
solvent	0
Protein residues	8514
RMS(bonds)	0.004
RMS(angles)	0.75
Ramachandran favored (%)	92.32
Ramachandran allowed (%)	6.77
Ramachandran outliers (%)	0.92
Rotamer outliers (%)	3.78
Clashscore	13.49
Average B-factor	124.08
macromolecules	124.08

METHODS

Subjects. One subject, a kidney transplant recipient with a history of allograft rejection and graft loss who was undergoing transplant nephrectomy was enrolled in this study at the University of Alabama at Birmingham (UAB) in 2021. This study was approved by the Institutional Review Board at UAB and informed consent was provided by the study subject. Additional data from brain-dead organ donors, deemed non-human subjects research, is also presented.

Multi-color flow cytometry and sorting. The allograft nephrectomy specimen was mechanically and enzymatically digested to yield a single cell suspension. Mononuclear cells were isolated from peripheral blood using density-gradient centrifugation. These cell suspensions were stained with the following anti-human secondary antibody reagents: CD19::V500 (BD 561121, clone HIB19), CD71::BV605 (BD 743306, clone M-A712), CXCR4::BV650 (BD 740599, clone 12G5), FcRL5::BV711 (BD 749603, clone 509F6), CD38::BV786 (BD 563964, clone HIT2), IgD::FITC (BD 555778), CD21::PerCP-Cy5.5 (Biolegend 354908, clone Bu32), CD11c::PE (Biolegend 337205, clone Bu15), CD27::PE-CF594 (BD 562297, clone M-T271), 7-AAD (BD 559925), CD3::PE-Cy5 (Biolegend 300310, clone HIT3a), CD14::PE-Cy5 (Invitrogen 15-0149-42, clone 61D3), CD16::PE-Cy5 (BD 555408, clone 3G8), CD56::PE-Cy5 (BD 555517, clone B159), FcRL4::PE-Cy7 (Biolegend 340207, clone 413D12), CXCR5::AF700 (Biolegend 356916, clone J252D5), IgG::APC-H7 (BD 561297, clone G18-145). Cells were also stained with fluorescently labeled tetramers of recombinant HLA-A*01:01 (NIH tetramer core, in BV421 and AF647). Cells were sorted on a FACSAria (BD Biosciences) in the UAB Comprehensive Flow Cytometry Core as single cells for recombinant monoclonal expression and in bulk populations for next generation IgH sequencing.

Next generation sequencing of the IgH repertoire. After sorting B cells subsets directly into RLT buffer with 1% mercaptoethanol, lysates were snap frozen on dry ice and stored at -80°C. Total cellular RNA was extracted from bulk sorted B cell and ASC subsets with an RNeasy Micro kit (Qiagen) according to manufacturer's protocol, followed by reverse transcription, generation of DNA amplicons, indexing, library generation, and single-strand sequencing on a Miseq (Illumina).(Tipton et al., 2015)

Bioinformatics analysis of NGS data. IgH sequencing data were processed and analyzed as described previously.(Tipton et al., 2015) Joined paired-end read were assembled and quality filtered, using FastQC. Using IMGT/HighV-QUEST,(Lefranc et al., 2015) sequences were annotated, and "productive" sequences were utilized for downstream analyses. Sequences were clustered into lineages based upon V_H and J_H gene identity, identical HCDR3 length, and HCDR3 nucleotide identity >85%. Downstream analyses were performed in Matlab (R202a, The Mathworks Inc.).

Single cell recombinant antibody closing, sequencing, and expression. Single HLA-A*01:01 tetramer^{++} B cells were index-sorted into hypotonic lysis buffer in 384-well plates and stored at -80°C. cDNA was generated, and PCR amplicons were cloned into expression vectors containing the constant regions of human IgG1, IgK, or IgL. Plasmids were sequenced by Sanger sequencing. Plasmids of heavy and light chains were co-transfected using polyethyleneimine into 293FreeStyle cells (Invitrogen). Supernatants were screened for anti-HLA reactivity using cytometric bead arrays described below. rmAbs were then purified using Sepharose G Fast Flow (Cytiva) and rmAb concentrations were determined by UV spectrophotometry (Nanodrop, Thermo Fisher). For structural analysis by x-ray crystallography and cryo-electron microscopy, we subcloned the VDJ and VJ gene segments from the JTK191B_E07, JTK191B_L02, and JTK191B_M07 rmAbs and expressed each of these as antigen-binding fragments (Fabs) and purified these using CaptureSelect IgG-CH1 Affinity Matrix (Thermo Scientific).

Immunogenetic analysis of recombinant monoclonal antibodies. IgH and IgK/L sequences were submitted to IMGT/HighV-Quest at the time of preparation of this manuscript. Lineages were assigned based upon V_H, D_H, J_H, $V_{K/L}$, $J_{K/L}$ gene assignments, identical HCDR3 and LCDR3 lengths, and >85% NT identity across the HCDR3. In the case that multiple rmAbs shared all features except for the HCDR3 >85% identity, these rmAbs were manually assigned into the same lineage.

Generation of unmutated common ancestors for recombinant monoclonal antibodies. Unmutated common ancestors (UCAs) were generated by taking the reference sequence of each gene segment allele – V_H, D_H, J_H, $V_{K/L}$, $J_{K/L}$ as annotated by IMGT/HighV-QUEST and reverting all mutated residues to the reference, or germline, configuration. Nontemplated nucleotides (N-additions) were not modified. Amino acid sequences were provided to Sino Biological, which synthesized recombinant human IgG1 monoclonal antibodies of the UCA sequences.

Phylogenetic analysis. Trees were constructed using Phylip's DNA parsimony (dnapars) tool (v3.695; adjusting settings 1, 4, 5, 6 and O setting the germline sequence as the outgroup.(Felsenstein, 1993)

Plasma immunoglobulin proteomics. Plasma from the kidney transplant recipient was first affinity purified on an HLA-A*01:01 column. Plasma immunoglobulins were subjected to trypsin digest and peptides were analyzed by liquid chromatography tandem mass spectrometry (LC-MS/MS). MS-derived peptide amino acid (aa) sequences were used to probe a RepSeq database including all BCR sequences derived from the kidney, blood and rmAb IgH libraries and an unrelated large RepSeq dataset. Exact peptide matches to lineage sequences were determined and members of the lineages were ranked by % aa matched of total. Peptide sequences are plotted by position within IgH sequence and colored by the frequency of matches across the data set.

HLA cytometric bead arrays. HLA-coated microbeads (OneLambda, ThermoFisher) were incubated with single recombinant monoclonal IgG1 antibodies diluted to 10ug/mL in PBS for 15 minutes. Following incubation and washing, beads were then incubated with anti-IgG::AF488 in PBS with 1% BSA for 15 minutes. After a final wash step, beads were suspended in PBS and samples were run on a Cytoflex flow cytometer (Beckman Coulter Lifes Sciences). Data were analyzed in FlowJo and geometric mean fluorescence intensities of each HLA allele-specific microbead were calculated.

High-throughput localized surface plasmon resonance. Localized surface plasmon resonance (L-SPR) data were collected through single-cycle kinetic analyses against either recombinant, biotinylated HLA-A*01:01 or HLA-A*24:02. Based upon binding by cytometric bead array (above), rmAbs were selected for L-SPR studies. Data were collected using a 1:1 referencing system on the Nicoya Alto HT-SPR instrument, using carboxyl-coated sensors as described previously.(Woodruff et al., 2022) Biotinylated HLA-A*01:01 was suspended in phosphate-buffered saline (PBS) with 0.05% Tween-20 at 500ug/mL. Biotinylated HLA-A*24:02 was suspended in PBS with 0.05% Tween-20 at 200ug/mL. Each was immobilized on an EDC/NHS-activated carboxyl sensor for 20 minutes. rmAbs were diluted to 1.3uM in PBS with 0.05% Tween-20. Single-cycle kinetics were performed with five threefold analyte dilutions, with maximum concentrations of 433nM and interactions were collected at 25°C. Kinetic fitting was performed using a 1:1 Langmuir model within the Nicoya user portal, or for certain rmAbs poorly fit with a 1:1 Langmuir model, an affinity fit model was used (TraceDrawer, Ridgeview Instruments). rmAbs with responses below 50 plasmon resonance response units were judged to not have measurable binding by L-SPR.

Recombinant protein synthesis. We expressed and re-folded recombinant HLA-A*01:01 and HLA-A*24:02 using plasmids from the NIH Tetramer Core Facility and suitable peptides.(Altman and Davis, 2003; Chatzileontiadou et al., 2021; Garboczi et al., 1992)

X-ray crystallography and CryoEM: sample preparation. The recombinant folded HLA was purified, mixed with the Fab (1:1 molar ratio for E07/A*01:01) or with 2 Fabs (1:1:1 for L02/M07/A*01:01) to generate complexes, and purified again using size-exclusion chromatography. Complexes were then concentrated and prepared for subsequent structural studies. Concentrated E07 Fabs were mixed with HLA-A*01:01 on ice at a 1:1 ratio. Fab-HLA complexes were purified by size-exclusion chromatography on a Superdex S200 column in PBS.

X-ray crystallography: crystallization, data collection, structure determination, and refinement. Purified E07/A*01:01 complexes were concentrated to 9.8mg/mL and screened for crystallization conditions against commercially available kits using a Mosquito liquid handling robot (SPT Labtech). Crystallization conditions were optimized, and diffraction quality crystals were grown in 1.015 M sodium citrate tribasic dihydrate, 0.1 M

sodium cacodylate pH 6.5 at a 1:1 ratio of protein to precipitating agent. Crystals were cryo-protected in crystallization solution supplemented with 20% (v/v) ethylene glycol and frozen. Diffraction data was collected at SER-CAT beamline 22-ID and processed with HKL2000.(Otwinowski and Minor, 1997) Crystals exhibited a pseudo-cubic symmetry but had true C2 symmetry. Initial phases were solved by molecular replacement with PHASER (McCoy et al., 2007) using prior models of HLA (pdb ID: 6AT9),(Toor et al., 2018) antibody domains: VH (pdb ID: 6PZH),(Zhu et al., 2019) VL (pdb ID: 4HK0),(Schmidt et al., 2013) CH1 (pdb ID: 6AZZ).(Scally et al., 2017) After identifying a trimeric assembly of HLA-Fab complexes, the assembly was used to find three addition copies of the assembly, yielding an asymmetric unit that contained 12 copies of HLA and 12 copies of the Fab. Models were iteratively rebuilt with COOT (Emsley et al., 2010) and refined with phenix.refine.(Adams et al., 2010) Data collection and refinement statistics are attached (Table 1). Though 12 copies of each protein could be identified in the asymmetric unit, domain a3 for some HLA and b2m had degenerate density following refinement and were removed from the final model. After removal, Fo-Fc difference maps show some density for the additional domains, but they could not be accurately placed. The final model contains eight copies of the complete HLA-Fab complex, four additional copies with Fabs bound to HLA domain a3 and b2m removed. Structure factors and final refined coordinates will be deposited in the PDB with updated accession code.

CryoEM analysis: Grid preparation, data collection, and processing.
The L02/M07/A*01:01 complex was concentrated to 3.04 mg/mL in PBS. mGrids for electron cryomicroscopy were prepared by placing 3ul of solution on a 2/1-3T C-flat grid (Thick carbon, 300 mesh, Protochips), which was plunged into liquid ethane with a Mark IV vitrobot. The grids were clipped and transferred to a G3 FEI-Krios electron microscope at La Jolla Institute for Immunology. The Krios is equipped with a Gatan Bio-quantum energy filter with a 20eV slit. The images were detected on a K3 camera in counting mode (not super-resolution). The electron beam intensity was ~15e/pixel*s and 50 fractions were collected for every image, giving the specimen 1e/A*A*frame. The beam size was 900nm, which allowed us to collect 6 images per hole in the sample. The images were pre-processed with Warp, (Tegunov and Cramer, 2019) where the images were corrected for movement, their CTF parameters estimated, and an initial set of particles were picked.

CryoEM analysis: Model building and refinement. 3D reconstruction was performed using RELION-3.(Zivanov et al., 2018) Following particle picking, 2D classification, and ab initio model generation, a final reconstruction was reached at 3.14Å resolution. Maps were sharpened using RELION-3 and starting models were generating using AlphaFold (Jumper et al., 2021) within ChimeraX.(Pettersen et al., 2021) Models were checked in Molprobity.(Chen et al., 2010)

Structural analyses. Properties of Fab/HLA binding interfaces were analyzed using UCSF ChimeraX.(Pettersen et al., 2021) We identified interacting residues at the Fab:HLA interface using a heavy-atom (non-hydrogen atom) distance cutoff of <5Å.(Akbar et al., 2021) Epitopic residues were defined as those with an interatomic distance between a heavy atom in the Fab and a heavy atom in the HLA complex <5Å or any residues in the HLA complex with solvent accessible surface area that was buried in the formation of the Fab/HLA interface.

Immunoflourescent histology of allograft specimens. After obtaining the transplant nephrectomy specimen, sections were embedded in Tissue-Tek O.C.T. Compound (Sakura) and frozen in liquid nitrogen. Tissue sectioning was performed on a cryotome, and sections were stained with three different panels of anti-human secondary antibodies, including CD21::FITC (Biolegend 354910, clone Bu32), CD19::APC (BD 555415, clone HIB19), CD21::FITC (Biolegend 354910, clone Bu32), CD4::AF488 (Biolegend 317419, clone OKT4), CD19::PE (Biolegend 302208, clone HIB19), Ki67::APC (Biolegend 350514, clone Ki-67), anti-Ig::AF488 (Southern Biotech 2010-30, polyclonal), CD38::APC (Biolegend 305510, clone HIT2), and DAPI. Images were acquired on a Nikon Eclipse Ti microscope using the 20x objective.

Statistical analyses. Statistical comparisons of an observed distribution with the expected distribution were performed using the binomial test and the confidence interval of the proportion was calculated using the hybrid Wilson/Brown method in Prism (GraphPad Software). Spearman correlations were used to assess association between two nonparametric variables.

HLA typing by next-generation sequencing. HLA typing of both donor and recipient were performed by the UAB Histocompatibility Laboratory using its standard clinical assay for next-generation sequencing. Genomic DNA was extracted from peripheral blood samples using the Qiagen EZ1 DNA blood kit via the Buffy coat protocol. Library construction and enrichment were performed per manufacturer's protocols for the CareDx AlloSeq Tx 17 assay and libraries were run on the Illumina MiSeq. Propietary CareDx software, AlloSeq Assign, v1.0.3 (CareDX, Stockholm, Sweden) utilized references from the Immuno Polymorphism Database-ImMunoGeneTics project/HLA Database (IPD-IMGT/HLA database) v3.47.0.0 to make allele assignments for all HLA Class I and Class II loci.

REFERENCES

Adams, P.D., Afonine, P.V., Bunkoczi, G., Chen, V.B., Davis, I.W., Echols, N., Headd, J.J., Hung, L.W., Kapral, G.J., Grosse-Kunstleve, R.W.*, et al.* (2010). PHENIX: a comprehensive Python-based system for macromolecular structure solution. Acta Crystallogr D Biol Crystallogr *66*, 213-221.
Akbar, R., Robert, P.A., Pavlovic, M., Jeliazkov, J.R., Snapkov, I., Slabodkin, A., Weber, C.R., Scheffer, L., Miho, E., Haff, I.H.*, et al.* (2021). A compact vocabulary of paratope-epitope interactions enables predictability of antibody-antigen binding. Cell Rep *34*, 108856.
Altman, J.D., and Davis, M.M. (2003). MHC-peptide tetramers to visualize antigen-specific T cells. Curr Protoc Immunol *Chapter 17*, Unit 17 13.
Angeletti, D., Gibbs, J.S., Angel, M., Kosik, I., Hickman, H.D., Frank, G.M., Das, S.R., Wheatley, A.K., Prabhakaran, M., Leggat, D.J.*, et al.* (2017). Defining B cell immunodominance to viruses. Nat Immunol *18*, 456-463.
Asano, Y., Daccache, J., Jain, D., Ko, K., Kinloch, A., Veselits, M., Wolfgeher, D., Chang, A., Josephson, M., Cunningham, P.*, et al.* (2021). Innate-like self-reactive B cells infiltrate human renal allografts during transplant rejection. Nat Commun *12*, 4372.
Bezstarosti, S., Bakker, K.H., Kramer, C.S.M., de Fijter, J.W., Reinders, M.E.J., Mulder, A., Claas, F.H.J., and Heidt, S. (2021). A Comprehensive Evaluation of the Antibody-Verified Status of Eplets Listed in the HLA Epitope Registry. Front Immunol *12*, 800946.
Bezstarosti, S., Kramer, C.S.M., Claas, F.H.J., de Fijter, J.W., Reinders, M.E.J., and Heidt, S. (2022). Implementation of molecular matching in transplantation requires further characterization of both immunogenicity and antigenicity of individual HLA epitopes. Hum Immunol *83*, 256-263.
Callemeyn, J., Lerut, E., de Loor, H., Arijs, I., Thaunat, O., Koenig, A., Meas-Yedid, V., Olivo-Marin, J.C., Halloran, P., Chang, J.*, et al.* (2020). Transcriptional Changes in Kidney Allografts with Histology of Antibody-Mediated Rejection without Anti-HLA Donor-Specific Antibodies. J Am Soc Nephrol *31*, 2168-2183.
Chang, A., Henderson, S.G., Brandt, D., Liu, N., Guttikonda, R., Hsieh, C., Kaverina, N., Utset, T.O., Meehan, S.M., Quigg, R.J.*, et al.* (2011). In situ B cell-mediated immune responses and tubulointerstitial inflammation in human lupus nephritis. J Immunol *186*, 1849-1860.
Chatzileontiadou, D.S.M., Szeto, C., Jayasinghe, D., and Gras, S. (2021). Protein purification and crystallization of HLA-A *02:01 in complex with SARS-CoV-2 peptides. STAR Protoc *2*, 100635.
Chen, V.B., Arendall, W.B., 3rd, Headd, J.J., Keedy, D.A., Immormino, R.M., Kapral, G.J., Murray, L.W., Richardson, J.S., and Richardson, D.C. (2010). MolProbity: all-atom structure validation for macromolecular crystallography. Acta Crystallogr D Biol Crystallogr *66*, 12-21.
Cheng, J., Torkamani, A., Grover, R.K., Jones, T.M., Ruiz, D.I., Schork, N.J., Quigley, M.M., Hall, F.W., Salomon, D.R., and Lerner, R.A. (2011). Ectopic B-cell clusters that infiltrate transplanted human kidneys are clonal. Proc Natl Acad Sci U S A *108*, 5560-5565.
Clotet-Freixas, S., Kotlyar, M., McEvoy, C.M., Pastrello, C., Rodriguez-Ramirez, S., Farkona, S., Cardinal, H., Dieude, M., Hebert, M.J., Li, Y.*, et al.* (2021). Increased Autoantibodies Against Ro/SS-A, CENP-B, and La/SS-B in Patients With Kidney Allograft Antibody-mediated Rejection. Transplant Direct *7*, e768.
Duquesnoy, R.J. (2006). A structurally based approach to determine HLA compatibility at the humoral immune level. Hum Immunol *67*, 847-862.
Duquesnoy, R.J., Marrari, M., Mulder, A., Sousa, L.C., da Silva, A.S., and do Monte, S.J. (2014). First report on the antibody verification of HLA-ABC epitopes recorded in the website-based HLA Epitope Registry. Tissue Antigens *83*, 391-400.
Einecke, G., Sis, B., Reeve, J., Mengel, M., Campbell, P.M., Hidalgo, L.G., Kaplan, B., and Halloran, P.F. (2009). Antibody-mediated microcirculation injury is the major cause of late kidney transplant failure. Am J Transplant *9*, 2520-2531.
Emsley, P., Lohkamp, B., Scott, W.G., and Cowtan, K. (2010). Features and development of Coot. Acta Crystallogr D Biol Crystallogr *66*, 486-501.
Everly, M.J., Rebellato, L.M., Haisch, C.E., Ozawa, M., Parker, K., Briley, K.P., Catrou, P.G., Bolin, P., Kendrick, W.T., Kendrick, S.A.*, et al.* (2013). Incidence and impact of de novo donor-specific alloantibody in primary renal allografts. Transplantation *95*, 410-417.
Felsenstein, J. (1993). PHYLIP (phylogeny inference package), version 3.5 c (Joseph Felsenstein.).

Ferdman, J., Porcheray, F., Gao, B., Moore, C., DeVito, J., Dougherty, S., Thomas, M.V., Farkash, E.A., Elias, N., Kawai, T.*, et al.* (2014). Expansion and somatic hypermutation of B-cell clones in rejected human kidney grafts. Transplantation *98*, 766-772.
Garboczi, D.N., Hung, D.T., and Wiley, D.C. (1992). HLA-A2-peptide complexes: refolding and crystallization of molecules expressed in Escherichia coli and complexed with single antigenic peptides. Proc Natl Acad Sci U S A *89*, 3429-3433.
Gaston, R.S., Cecka, J.M., Kasiske, B.L., Fieberg, A.M., Leduc, R., Cosio, F.C., Gourishankar, S., Grande, J., Halloran, P., Hunsicker, L.*, et al.* (2010). Evidence for antibody-mediated injury as a major determinant of late kidney allograft failure. Transplantation *90*, 68-74.
Gu, Y., Wong, Y.H., Liew, C.W., Chan, C.E.Z., Murali, T.M., Yap, J., Too, C.T., Purushotorman, K., Hamidinia, M., El Sahili, A.*, et al.* (2019). Defining the structural basis for human alloantibody binding to human leukocyte antigen allele HLA-A*11:01. Nat Commun *10*, 893.
Hill, J.A., Kiem, E.S., Bhatti, A., Liu, W., Keane-Candib, J., Fitzpatrick, K.S., Boonyaratanakornkit, J., Gardner, R.A., Green, D.J., Maloney, D.G.*, et al.* (2023). Anti-HLA antibodies in recipients of CD19 versus BCMA-targeted CAR T-cell therapy. Am J Transplant *23*, 416-422.
Hippen, B.E., DeMattos, A., Cook, W.J., Kew, C.E., 2nd, and Gaston, R.S. (2005). Association of CD20+ infiltrates with poorer clinical outcomes in acute cellular rejection of renal allografts. Am J Transplant *5*, 2248-2252.
Honger, G., Niemann, M., Schawalder, L., Jones, J., van Heck, M.R., van de Pasch, L.A.L., Vendelbosch, S., Rozemuller, E.H., Hosli, I., Blumel, S.*, et al.* (2020). Toward defining the immunogenicity of HLA epitopes: Impact of HLA class I eplets on antibody formation during pregnancy. HLA.
Jumper, J., Evans, R., Pritzel, A., Green, T., Figurnov, M., Ronneberger, O., Tunyasuvunakool, K., Bates, R., Zidek, A., Potapenko, A.*, et al.* (2021). Highly accurate protein structure prediction with AlphaFold. Nature *596*, 583-589.
Kajander, T., Kahn, P.C., Passila, S.H., Cohen, D.C., Lehtio, L., Adolfsen, W., Warwicker, J., Schell, U., and Goldman, A. (2000). Buried charged surface in proteins. Structure *8*, 1203-1214.
Kwak, K., Quizon, N., Sohn, H., Saniee, A., Manzella-Lapeira, J., Holla, P., Brzostowski, J., Lu, J., Xie, H., Xu, C.*, et al.* (2018). Intrinsic properties of human germinal center B cells set antigen affinity thresholds. Sci Immunol *3*.
Lee, Y.H., Sato, Y., Saito, M., Fukuma, S., Saito, M., Yamamoto, S., Komatsuda, A., Fujiyama, N., Satoh, S., Lee, S.H.*, et al.* (2022). Advanced Tertiary Lymphoid Tissues in Protocol Biopsies are Associated with Progressive Graft Dysfunction in Kidney Transplant Recipients. J Am Soc Nephrol *33*, 186-200.
Lefranc, M.P., Giudicelli, V., Duroux, P., Jabado-Michaloud, J., Folch, G., Aouinti, S., Carillon, E., Duvergey, H., Houles, A., Paysan-Lafosse, T.*, et al.* (2015). IMGT(R), the international ImMunoGeneTics information system(R) 25 years on. Nucleic Acids Res *43*, D413-422.
Liarski, V.M., Kaverina, N., Chang, A., Brandt, D., Yanez, D., Talasnik, L., Carlesso, G., Herbst, R., Utset, T.O., Labno, C.*, et al.* (2014). Cell distance mapping identifies functional T follicular helper cells in inflamed human renal tissue. Sci Transl Med *6*, 230ra246.
Louis, K., Bailly, E., Macedo, C., Lau, L., Ramaswami, B., Chang, A., Chandran, U., Landsittel, D., Gu, X., Chalasani, G.*, et al.* (2021). T-bet+CD27+CD21- B cells poised for plasma cell differentiation during antibody-mediated rejection of kidney transplants. JCI Insight *6*.
Lu, S., Xie, X.X., Zhao, L., Wang, B., Zhu, J., Yang, T.R., Yang, G.W., Ji, M., Lv, C.P., Xue, J.*, et al.* (2021). The immunodominant and neutralization linear epitopes for SARS-CoV-2. Cell Rep *34*, 108666.
Luque, S., Lucia, M., Melilli, E., Lefaucheur, C., Crespo, M., Loupy, A., Bernal-Casas, D., Goma, M., Jarque, M., Crespo, E.*, et al.* (2019). Value of monitoring circulating donor-reactive memory B cells to characterize antibody-mediated rejection after kidney transplantation. Am J Transplant *19*, 368-380.
Marcu, A., Bichmann, L., Kuchenbecker, L., Kowalewski, D.J., Freudenmann, L.K., Backert, L., Muhlenbruch, L., Szolek, A., Lubke, M., Wagner, P.*, et al.* (2021). HLA Ligand Atlas: a benign reference of HLA-presented peptides to improve T-cell-based cancer immunotherapy. J Immunother Cancer *9*.
McCoy, A.J., Grosse-Kunstleve, R.W., Adams, P.D., Winn, M.D., Storoni, L.C., and Read, R.J. (2007). Phaser crystallographic software. J Appl Crystallogr *40*, 658-674.
Mei, H.E., Frolich, D., Giesecke, C., Loddenkemper, C., Reiter, K., Schmidt, S., Feist, E., Daridon, C., Tony, H.P., Radbruch, A.*, et al.* (2010). Steady-state generation of mucosal IgA+ plasmablasts is not abrogated by B-cell depletion therapy with rituximab. Blood *116*, 5181-5190.

Merrill, J.P., Murray, J.E., Harrison, J.H., and Guild, W.R. (1956). Successful homotransplantation of the human kidney between identical twins. J Am Med Assoc *160*, 277-282.
Moreso, F., Crespo, M., Ruiz, J.C., Torres, A., Gutierrez-Dalmau, A., Osuna, A., Perello, M., Pascual, J., Torres, I.B., Redondo-Pachon, D.*, et al.* (2018). Treatment of chronic antibody mediated rejection with intravenous immunoglobulins and rituximab: A multicenter, prospective, randomized, double-blind clinical trial. Am J Transplant *18*, 927-935.
Otwinowski, Z., and Minor, W. (1997). Processing of X-ray diffraction data collected in oscillation mode. Methods Enzymol *276*, 307-326.
Perry, D.K., Pollinger, H.S., Burns, J.M., Rea, D., Ramos, E., Platt, J.L., Gloor, J.M., and Stegall, M.D. (2008). Two novel assays of alloantibody-secreting cells demonstrating resistance to desensitization with IVIG and rATG. Am J Transplant *8*, 133-143.
Pettersen, E.F., Goddard, T.D., Huang, C.C., Meng, E.C., Couch, G.S., Croll, T.I., Morris, J.H., and Ferrin, T.E. (2021). UCSF ChimeraX: Structure visualization for researchers, educators, and developers. Protein Sci *30*, 70-82.
Porcheray, F., DeVito, J., Helou, Y., Dargon, I., Fraser, J.W., Nobecourt, P., Ferdman, J., Germana, S., Girouard, T.C., Kawai, T.*, et al.* (2012). Expansion of polyreactive B cells cross-reactive to HLA and self in the blood of a patient with kidney graft rejection. Am J Transplant *12*, 2088-2097.
Ramaraj, T., Angel, T., Dratz, E.A., Jesaitis, A.J., and Mumey, B. (2012). Antigen-antibody interface properties: composition, residue interactions, and features of 53 non-redundant structures. Biochim Biophys Acta *1824*, 520-532.
Roufosse, C., Simmonds, N., Clahsen-van Groningen, M., Haas, M., Henriksen, K.J., Horsfield, C., Loupy, A., Mengel, M., Perkowska-Ptasinska, A., Rabant, M.*, et al.* (2018). A 2018 Reference Guide to the Banff Classification of Renal Allograft Pathology. Transplantation *102*, 1795-1814.
Saini, D., Weber, J., Ramachandran, S., Phelan, D., Tiriveedhi, V., Liu, M., Steward, N., Aloush, A., Hachem, R., Trulock, E.*, et al.* (2011). Alloimmunity-induced autoimmunity as a potential mechanism in the pathogenesis of chronic rejection of human lung allografts. J Heart Lung Transplant *30*, 624-631.
Scally, S.W., McLeod, B., Bosch, A., Miura, K., Liang, Q., Carroll, S., Reponen, S., Nguyen, N., Giladi, E., Ramisch, S.*, et al.* (2017). Molecular definition of multiple sites of antibody inhibition of malaria transmission-blocking vaccine antigen Pfs25. Nat Commun *8*, 1568.
Schinstock, C.A., Mannon, R.B., Budde, K., Chong, A.S., Haas, M., Knechtle, S., Lefaucheur, C., Montgomery, R.A., Nickerson, P., Tullius, S.G.*, et al.* (2020). Recommended Treatment for Antibody-mediated Rejection After Kidney Transplantation: The 2019 Expert Consensus From the Transplantion Society Working Group. Transplantation *104*, 911-922.
Schmidt, A.G., Xu, H., Khan, A.R., O'Donnell, T., Khurana, S., King, L.R., Manischewitz, J., Golding, H., Suphaphiphat, P., Carfi, A.*, et al.* (2013). Preconfiguration of the antigen-binding site during affinity maturation of a broadly neutralizing influenza virus antibody. Proc Natl Acad Sci U S A *110*, 264-269.
Sellares, J., de Freitas, D.G., Mengel, M., Reeve, J., Einecke, G., Sis, B., Hidalgo, L.G., Famulski, K., Matas, A., and Halloran, P.F. (2012). Understanding the causes of kidney transplant failure: the dominant role of antibody-mediated rejection and nonadherence. Am J Transplant *12*, 388-399.
Senev, A., Coemans, M., Lerut, E., Van Sandt, V., Kerkhofs, J., Daniels, L., Driessche, M.V., Compernolle, V., Sprangers, B., Van Loon, E.*, et al.* (2020). Eplet Mismatch Load and De Novo Occurrence of Donor-Specific Anti-HLA Antibodies, Rejection, and Graft Failure after Kidney Transplantation: An Observational Cohort Study. J Am Soc Nephrol *31*, 2193-2204.
Senev, A., Lerut, E., Coemans, M., Callemeyn, J., Copley, H.C., Claas, F., Koshy, P., Kosmoliaptsis, V., Kuypers, D., Sprangers, B.*, et al.* (2022). Association of HLA Mismatches and Histology Suggestive of Antibody-Mediated Injury in the Absence of Donor-Specific Anti-HLA Antibodies. Clin J Am Soc Nephrol *17*, 1204-1215.
Tambur, A.R., and Das, R. (2022). Can We Use Eplets (or Molecular) Mismatch Load Analysis to Improve Organ Allocation? The Hope and the Hype. Transplantation.
Tegunov, D., and Cramer, P. (2019). Real-time cryo-electron microscopy data preprocessing with Warp. Nat Methods *16*, 1146-1152.
Tipton, C.M., Fucile, C.F., Darce, J., Chida, A., Ichikawa, T., Gregoretti, I., Schieferl, S., Hom, J., Jenks, S., Feldman, R.J.*, et al.* (2015). Diversity, cellular origin and autoreactivity of antibody-secreting cell population expansions in acute systemic lupus erythematosus. Nat Immunol *16*, 755-765.

Toor, J.S., Rao, A.A., McShan, A.C., Yarmarkovich, M., Nerli, S., Yamaguchi, K., Madejska, A.A., Nguyen, S., Tripathi, S., Maris, J.M.*, et al.* (2018). A Recurrent Mutation in Anaplastic Lymphoma Kinase with Distinct Neoepitope Conformations. Front Immunol *9*, 99.
Tsai, E.W., Rianthavorn, P., Gjertson, D.W., Wallace, W.D., Reed, E.F., and Ettenger, R.B. (2006). CD20+ lymphocytes in renal allografts are associated with poor graft survival in pediatric patients. Transplantation *82*, 1769-1773.
Turner, J.S., Zhou, J.Q., Han, J., Schmitz, A.J., Rizk, A.A., Alsoussi, W.B., Lei, T., Amor, M., McIntire, K.M., Meade, P.*, et al.* (2020). Human germinal centres engage memory and naive B cells after influenza vaccination. Nature *586*, 127-132.
Wardemann, H., Yurasov, S., Schaefer, A., Young, J.W., Meffre, E., and Nussenzweig, M.C. (2003). Predominant autoantibody production by early human B cell precursors. Science *301*, 1374-1377.
Wehmeier, C., Karahan, G.E., Krop, J., de Vaal, Y., Langerak-Langerak, J., Binet, I., Schaub, S., Roelen, D.L., Claas, F.H.J., Heidt, S.*, et al.* (2019). Donor-specific B cell memory in alloimmunized kidney transplant recipients - first clinical application of a novel method. Transplantation.
Wiebe, C., Gibson, I.W., Blydt-Hansen, T.D., Karpinski, M., Ho, J., Storsley, L.J., Goldberg, A., Birk, P.E., Rush, D.N., and Nickerson, P.W. (2012). Evolution and clinical pathologic correlations of de novo donor-specific HLA antibody post kidney transplant. Am J Transplant *12*, 1157-1167.
Wiebe, C., Pochinco, D., Blydt-Hansen, T.D., Ho, J., Birk, P.E., Karpinski, M., Goldberg, A., Storsley, L.J., Gibson, I.W., Rush, D.N.*, et al.* (2013). Class II HLA epitope matching-A strategy to minimize de novo donor-specific antibody development and improve outcomes. Am J Transplant *13*, 3114-3122.
Woodruff, M.C., Ramonell, R.P., Haddad, N.S., Anam, F.A., Rudolph, M.E., Walker, T.A., Truong, A.D., Dixit, A.N., Han, J.E., Cabrera-Mora, M.*, et al.* (2022). Dysregulated naive B cells and de novo autoreactivity in severe COVID-19. Nature *611*, 139-147.
Woodruff, M.C., Ramonell, R.P., Nguyen, D.C., Cashman, K.S., Saini, A.S., Haddad, N.S., Ley, A.M., Kyu, S., Howell, J.C., Ozturk, T.*, et al.* (2020). Extrafollicular B cell responses correlate with neutralizing antibodies and morbidity in COVID-19. Nat Immunol *21*, 1506-1516.
Yamauchi, O. (2016). Noncovalent interactions in biocomplexes. Physical Sciences Reviews *1*.
Zeng, Q., Ng, Y.H., Singh, T., Jiang, K., Sheriff, K.A., Ippolito, R., Zahalka, S., Li, Q., Randhawa, P., Hoffman, R.A.*, et al.* (2014). B cells mediate chronic allograft rejection independently of antibody production. J Clin Invest *124*, 1052-1056.
Zhang, H., Cavazzoni, C.B., Hanson, B.L., Bechu, E.D., Podesta, M.A., Azzi, J., Blazar, B.R., Chong, A.S., Kreisel, D., Alessandrini, A.*, et al.* (2023). Transcriptionally Distinct B Cells Infiltrate Allografts After Kidney Transplantation. Transplantation *107*, e47-e57.
Zhang, Z., Schuster, S.J., Lacey, S.F., Milone, M.C., Monos, D., and Bhoj, V.G. (2020). Stable HLA antibodies following sustained CD19+ cell depletion implicate a long-lived plasma cell source. Blood Adv *4*, 4292-4295.
Zhu, X., Turner, H.L., Lang, S., McBride, R., Bangaru, S., Gilchuk, I.M., Yu, W., Paulson, J.C., Crowe, J.E., Jr., Ward, A.B.*, et al.* (2019). Structural Basis of Protection against H7N9 Influenza Virus by Human Anti-N9 Neuraminidase Antibodies. Cell Host Microbe *26*, 729-738 e724.
Zivanov, J., Nakane, T., Forsberg, B.O., Kimanius, D., Hagen, W.J., Lindahl, E., and Scheres, S.H. (2018). New tools for automated high-resolution cryo-EM structure determination in RELION-3. Elife *7*.